Food Hydrocolloids 166 (2025) 111330

Contents lists available at ScienceDirect

Food Hydrocolloids

journal homepage: www.elsevier.com/locate/foodhyd

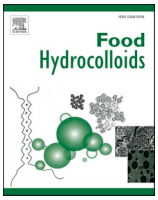

High internal phase emulsions stabilized by insect proteins: A path to 3D printable fat analogues

Aurélie Ballon [a], Sarah Sessa [a], Salvatore Cito [b], Sílvia de Lamo-Castellví [a,c], Carme Güell [a], Montse Ferrando [a,*]

[a] Departament d'Enginyeria Química, Escola Tècnica Superior d'Enginyeria Química, Universitat Rovira i Virgili, Avda. Països Catalans, 26, 43007, Tarragona, Spain
[b] Departament d'Enginyeria Mecànica, Universitat Rovira i Virgili, Escola Tècnica Superior d'Enginyeria Química, Av. Països Catalans 26, Tarragona, 43007, Spain
[c] Department of Food Science and Technology, The Ohio State University, 110 Parker Food Science and Technology Building, 2015 Fyffe Road, Columbus, OH, 43210, United States

ARTICLE INFO

Keywords:
Insect protein
High internal phase emulsions
Fat analogues
Edible food ink
3D printing

ABSTRACT

In response to the growing interest in plant oil-based adipose tissue analogues, high internal phase emulsions (HIPEs) stabilized with insect proteins from lesser mealworm (*Alphitobius diaperinus* larva) and house cricket (*Acheta domesticus*) were developed with the objective of making them 3D printable and able to imitate the gel-like structure of meat fat. To this end, the effect of thermal treatment on the properties of the proteins and the resulting HIPEs was investigated. The particle size, ζ-potential, and surface hydrophobicity of native and heat-treated insect proteins in suspension proved their potential to stabilize HIPEs. Thermal treatment altered protein structures (secondary and tertiary), leading to the formation of protein aggregates. HIPEs (80 wt% sunflower oil), stable during storage at room temperature, were successfully produced using protein dispersions at concentrations ranging from 0.5% to 3%. The rheological properties relevant to the various phases of three-dimensional printing were evaluated. All HIPEs exhibited elastic modulus (G') values that exceeded loss modulus (G'') values, indicating a predominant elastic behavior. The viscosity, yield stress, and recovery rates of HIPEs stabilized with thermally treated proteins were found to be higher than those of HIPEs stabilized with native proteins. The insect protein-stabilized HIPEs produced in this study displayed physical stability and rheological properties suitable for use as food ink, as evidenced by their successful printing into cylindrical shapes, which demonstrated good printability. These findings suggest that insect proteins have promising potential for use in stabilizing HIPEs as 3D printable fat analogues.

1. Introduction

Plant-based meat analogues are gaining popularity for environmental, ethical, and health reasons, although they have room for improvement in terms of organoleptic quality. The capacity to emulate adipose tissue has been identified as a key opportunity to enhance the resemblance of plant-based meat products to their animal-based counterparts, and consequently, to the sensory experience of consumers. A number of approaches have been proposed to create plant-based alternatives to adipose tissue to improve sensory properties of meat analogues. Among these are emulsion gels, which are solid-like emulsions made by gelling the continuous phase of a liquid-like emulsion or by aggregating the emulsion droplets (Czapalay & Marangoni, 2024). Concentrated oil-in-water emulsions can also be used to create semi-solid materials with a microstructure and appearance similar to that of beef or pork adipose tissue (Hu & McClements, 2022). An example of this is high internal phase emulsions (HIPEs) with an internal oil phase volume fraction that exceeds packing limit (74%, for the hexagonal close packing of monodisperse droplets) (Fuhrmann et al., 2022). These emulsions are no longer in a liquid state but become a soft solid with viscoelastic properties. They exhibit high resistance to coalescence, phase separation, lipid oxidation, and changes in environmental conditions, as well as high capacity for loading liposoluble compounds. Due to their unique properties, HIPEs have gained significant attention in the field of edible emulsions for the formulation and texturization of healthier products rich in unsaturated fatty acids, aiming to reduce lipid oxidation while replacing trans fats (Abdullah et al., 2020) and, more recently, to mimic adipose tissue (Hu & McClements,

* Corresponding author
E-mail address: montse.ferrando@urv.cat (M. Ferrando).

https://doi.org/10.1016/j.foodhyd.2025.111330
Received 3 December 2024; Received in revised form 14 February 2025; Accepted 6 March 2025
Available online 7 March 2025

2022). In addition, the ability of HIPEs to be 3D printed may benefit the development of a microstructure that more closely resembles adipose tissue (Wu et al., 2022; Zhang, Pandya, et al., 2022).

The suitability of a HIPE as food ink can be explored by studying the rheological properties. Indeed, the extrusion-based 3D printing process can be divided into three distinct stages, each requiring specific rheological properties (Li et al., 2023): i) in the extrusion stage, a smooth extrusion and continuous flow depend on the viscosity, shear-thinning behavior, and yield stress of the ink; ii) the ability of the ink to recover its viscosity and mechanical strength during the recovery stage can be measured by evaluating its shear and temperature recovery; iii) in the final self-support stage of 3D printing, the printed ink must have sufficient mechanical strength and high yield stress to maintain the shape and prevent layer collapse (Li et al., 2023; Liu et al., 2019).

Previously, HIPEs were stabilized with a combination of inorganic particles and large amounts of surfactants (5–50%), limiting their use in food products because of health and environment adverse effects (Ji & Luo, 2023). Therefore, research has focused on finding food-grade biopolymers (e.g., proteins, polysaccharides, and complexes) for stabilizing HIPEs. HIPEs stabilized by plant or animal proteins have already proven to be effective printable materials with high printing accuracy (Ji & Luo, 2023; Zhang et al., 2023).

Insect proteins are a sustainable alternative to conventional proteins since insect farming requires significantly less water and land and emits fewer greenhouse gases compared to conventional animal husbandry (dos Santos Aguilar, J.G., 2021; van Huis & Oonincx, 2017). Proteins extracted from several insect species were shown to have a comparable ability to stabilize oil-in-water (O/W) and water-in-oil-in-water (W/O/W) emulsions to dairy proteins, and an improved ability compared to plant proteins, such as pea protein (Wang, Ballon, et al., 2021; Wang, Jousse, et al., 2021). To date, two studies have investigated the use of insect proteins to stabilize HIPEs with promising results. Huang et al. (2022) reported that HIPEs (80% oil, v/v) stabilized with 0.5% or 2% (w/v) mealworm (*Tenebrio molitor*) protein showed great physical stability during storage at room temperature for 30 days. Moreover, silkworm (*Bombix mori*) pupae particles were produced by ultrasonic treatment near the isoelectric point, and were used to stabilize HIPEs (75% oil, v/v) that were stable until reaching the intestinal digestion stage enabling a target release of the oil phase (Jiang, Wang, et al., 2023).

The techno-functional properties of proteins, particularly the emulsifying properties, can be modified and/or improved by altering their structure or chemical groups, through physical, chemical, biological or other modification approaches (Nasrabadi et al., 2021). Physical modifications (e.g., thermal treatment, ultrafiltration, ultrasound, and high-pressure treatment) are gaining interest as they do not require the use of additional chemicals or enzymes. Thermal treatments promote proteins unfolding and further aggregation, for instance, black cricket (*Gryllus assimilis*) proteins, after thermal treatment (in presence or absence of NaCl), had improved foamability, foam stability, and gelling properties (Santiago et al., 2021).

The objective of this study was to investigate the potential of two different insect proteins, the lesser mealworm (larvae of *Alphitobius diaperinus*) and the house cricket (*Acheta domesticus*), both native and heat-treated, to develop HIPEs with a printability suitable for the design of adipose tissue analogues. None of these insect proteins, native or modified, have been ever assessed for this specific purpose. To fulfil the objective, HIPEs (80% w/w) stabilized with both native and thermally-treated insect proteins were systematically formulated, and the significant rheological properties for fabricating a well-defined printable ink were determined and compared with those exhibited by whey protein-stabilized HIPEs, which served as the benchmark protein in this case. Subsequently, HIPEs were 3D printed, after adjusting the conditions to align with their rheological behavior, and the shape definition and stability of the 3D-printed models was evaluated under refrigeration for 9 days. As far as the authors knowledge, this is the first attempt to structure insect-protein stabilized HIPEs by 3D printing, paving the way to their application as a potential adipose tissue analogue.

2. Materials and methods

2.1. Materials

Proteins used in this study include proteins extracted from edible lesser mealworm (*Alphitobius diaperinus* larva) powder (Kreca Ento-Food BV, Wageningen, the Netherlands), edible house cricket (*Acheta domesticus*) powder (Albinsecta, Werkhoven, the Netherlands), and whey protein isolate (WPI) which was kindly provided by Davisco Foods International (98.0% purity, Le Sueur, MN, USA). The defatting of the insect meals was carried out using 2-methyltetrahydrofuran (Scharlab, Barcelona, Spain). The pH of the solutions was adjusted using sodium hydroxide (NaOH) and hydrochloric acid (37%, HCl) purchased from Sigma-Aldrich (Saint Louis, MO, USA). The soluble protein content in solution was quantified using a Pierce™ BCA protein assay kit (ThermoFisher Scientific, Waltham, MA, USA). The concentrations were expressed in bovine serum albumin equivalent (BSAE%, w/w) and are shown in % for simplicity. Sodium azide (NaN_3), sodium chloride (NaCl), 8-anilino-1-naphthalenesulfonic acid (≥97%, ANS) were purchased from Sigma-Aldrich (Saint Louis, MO, USA). Sunflower oil (Borges S.A., Reus, Spain) was bought from a local supermarket. All reagents were analytical grade, and deionized water was used for the preparation of the samples and reagents.

2.2. Defatting and extraction of proteins

Lesser mealworm protein concentrate (LMPC) and cricket protein concentrate (CPC) were obtained following a method developed in the research group (Ballon et al., 2024) with some modifications. First, the powders were defatted, 50 g of powder was mixed with 250 mL of 2-methyltetrahydrofuran, a bio-based solvent, at 600 rpm for 1 h at room temperature. Subsequently, the mixture was left to decant until achieving complete phase separation. Following this, the solvent phase containing lipids was carefully removed. This process was repeated 3 times in total to ensure that all lipids were removed from the powder. Then, the sample was placed under a fume hood overnight to evaporate residual solvent.

The protein extraction was performed by alkaline solubilization followed by acid precipitation at their isoelectric point. To do so, the defatted insect powder was mixed with 0.25 M NaOH (ratio 1:5, w/v) and stirred at 400 rpm at 40 °C for 1 h. Afterwards, the mixture was centrifuged (3358×*g*, 15 min) and the supernatant was collected. The remaining pellet was used to repeat the process, which was performed a total of 3 times. The proteins from the supernatant were precipitated by adjusting the pH to 4.0–4.5 and the mixture was centrifuged (2343×*g*, 15 min). The precipitates were freeze-dried (LYOQUEST-85 PLUS, Telstar, Barcelona, Spain), ground, and stored in plastic bags at 4 °C in a desiccator.

2.3. Modification of proteins through heat treatment

The thermal treatment was performed according to Zhu et al. (2017) with some modifications. First, protein concentrates were dispersed in distilled water during 2 h (RCT ST, IKA, Staufen, Germany) and the pH of the dispersions was adjusted to 7.0 (Accumet® AE150, Fisher Scientific, Walthom, MA, USA). The dispersions were kept at 4 °C overnight to allow full hydration of the proteins. Then, the dispersions were centrifuged (Meditronic 7000599, J.P. SELECTA, Barcelona, Spain) at 2863×*g* for 15 min to remove the insoluble proteins. The protein content of the supernatant was determined using BCA assay and adjusted to 3.5% by dilution with distilled water. Then, sodium chloride was added to the protein solution while stirring, until reaching 300 mM. Sodium azide (0.02%) was added as well to prevent microbial growth. Aliquots of the

protein solution (2 mL) were pipetted into glass tubes and were heated in a dry bath (Digital shaking dry bath, Thermo Fisher Scientific, Waltham, MA, USA) at 90 °C for 30 min with low agitation (20 rpm). Afterwards, the tubes were cooled down in a water-ice bath during at least 30 min. The thermally-treated LMPC and CPC (LMPC-ThT and CPC-ThT, respectively) were used within one day following the preparation. Untreated (native) LMPC and CPC (LMPC-UnT and CPC-UnT, respectively) were used as control.

2.4. Characterization of the insect protein dispersions

2.4.1. Protein particle size and ζ-potential

The particle size distribution of the protein suspension was determined by laser diffraction using a Mastersizer 2000 (Malvern Instruments, Worcestershire, UK) following the method of Pinel et al. (2024) with slight modifications. A refractive index of 1.46 was chosen for the particles and 1.33 for the dispersant. The ζ-potential of the insect protein dispersions (untreated and treated) were measured at pH 7, using a Zetasizer Nano-ZS (Malvern Instruments, Worcestershire, UK) at 25 °C. The refractive index of the dispersant was set to 1.33. The ζ-potential was calculated using the Smoluchowski model. Measurements of particle size and ζ-potential were performed in triplicate.

2.4.2. Fourier transform mid-infrared (FT-MIR) spectroscopy

The secondary structures of both the untreated and thermally-treated proteins were studied using FT-MIR spectroscopy. Mid-infrared spectra were collected using an Agilent 4500 portable unit equipped with triple-reflection diamond attenuated total reflectance (ATR) crystal and thermoelectrically-cooled DTGS detector (Agilent Technologies Inc., Danbury, CT, USA). The diamond crystal ATR system had a 2 mm diameter sampling surface with a 200 μm active area. To perform the analysis, the protein solutions were vortexed and pipetted (5 μL) onto the ATR sampling window. The water was evaporated under vacuum until a film was obtained, to avoid the interferences. Each spectrum is the average of 128 scans of a 4 cm^{-1} resolution, co-added to improve the signal to noise ratio over the 4000–700 cm^{-1} range. Protein samples were prepared in triplicate and the spectra acquisition was repeated twice under the same conditions for each sample.

The relative percentage content of each secondary structure element was determined by curve fitting of the second derivative of the amide I region (1700–1600 cm^{-1}) following the procedure of Hackshaw et al. (2023) using OriginPro 2023 (Origin Lab, MA, Northampton, USA). The raw spectra (in the region 1700–1600 cm^{-1}) was first normalized ([0–100]) and then smoothed (Savitsky-Golay function, 5 points). The second derivative was calculated using a Savitsky-Golay function (9 points), multiplied by (−1) for visualization purposes and baseline-corrected. Finally, the spectra were fitted using the "Multiple Peak Fit" option (Chi-square tolerance value of 1×10^{-9}) and the area of the different peaks fitted was divided by the total area to obtain the relative area of each band. The wavelength of the bands was correlated with the secondary structures as follow: β-sheet (antiparallel: 1618–1637 cm^{-1} and parallel: 1682–1695 cm^{-1}), random coil (1637–1645 cm^{-1}), α-helix (1645–1662 cm^{-1}) and β-turn (1662–1682 cm^{-1}) (Gkinali et al., 2022).

2.4.3. Intrinsic fluorescence

The intrinsic fluorescence was measured using a Varian Cary Eclipse fluorescence spectrophotometer (Agilent, Santa Clara, CA, USA) according to the method described by Ballon et al. (2024). Briefly, the protein dispersions were diluted to 1 mg/mL protein using 10 mM phosphate buffer at pH 7.0. The exciting wavelength was set to 280 nm to target tryptophan and the emission spectra were measured in the range of 270–450 nm. The exciting and emission slit widths were set to 5 nm. Samples were measured in triplicate.

2.4.4. Surface hydrophobicity

Surface hydrophobicity (H_0) was determined using ANS as fluorescence probe using the method of Mishyna et al. (2019) with slight modifications. The protein dispersions were diluted in phosphate buffer (10 mM, pH 7.0) to prepare sample solutions of 0.005, 0.025, 0.05, and 0.1 mg protein/mL. Then 20 μL of ANS solution (8 mM) was added to 4 mL of each sample solution, the mixture was vortexed and kept in the dark for 15 min. The fluorescence intensity was measured using a fluorescence spectrophotometer (Varian Cary Eclipse fluorescence spectrophotometer, Agilent, Santa Clara, CA, USA) at excitation and emission wavelengths of 390 and 470 nm, respectively. The excitation and emission slit widths were set to 5 nm. The fluorescence intensity obtained for phosphate buffer was subtracted from all values. The protein surface hydrophobicity was determined as the slope of the linear regression of the fluorescence intensity against the protein concentration (mg/mL). All the samples were measured in triplicate.

2.5. Preparation of HIPEs

HIPEs were produced by mixing sunflower oil (80 wt%) with the untreated or thermally treated protein solution (20 wt%), containing 0.5%, 1%, 2%, and 3% protein, in a 50 mL plastic tube. The oil was slowly added to the protein solution while mixing at 15 000 rpm (Ultra Turrax T18 digital, IKA, Staufen, Germany). Once the oil was totally added, the mixture was homogenized for 2 more minutes. A minimum of two emulsions were prepared independently.

The type of emulsion (O/W or W/O) was determined by dispersing drops of emulsion in distilled water or sunflower oil. Emulsions dispersing easily in distilled water were considered as O/W emulsions.

2.6. Characterization of HIPEs

2.6.1. Visual appearance and optical microscopy

The emulsions were placed in glass tubes and pictures were taken with the tube straight and upside-down. The HIPE microstructure was visualized at ambient temperature using an inverted microscope (Primovert, Carl Zeiss AG, Oberkochen, Germany) under a 40x objective, equipped with a camera (SpeedCam MacroVis EoSens, High Speed Vision GmbH, Ettlingen, Germany).

2.6.2. Droplet size distribution

The droplet size distribution of emulsions was analyzed by laser diffraction using a Mastersizer 2000 (Malvern Instruments, Worcestershire, UK). Refractive index was set to 1.472 and 1.330 for sunflower oil and water, respectively. The emulsions were diluted around 10 times using deionized water or 1% (w/w) SDS solution before the measurement. Emulsion droplets can flocculate and a simple dilution in water can disrupt weakly flocculated droplets but let intact stronger ones. By dispersing the emulsions in SDS solution, the flocs can be disassembled. Therefore, measuring both in water and SDS allows assessing the size of flocs stable in the measuring conditions, and the real droplet size of the emulsions, respectively (Palazolo et al., 2011).

The mean droplet size and droplet size distribution width was reported as volume-weighted mean diameter ($d_{4,3}$) and span, calculated according to Equation (1) and Equation (2), respectively.

$$d_{4,3} = \frac{\sum n_i \bullet d_i^4}{\sum n_i \bullet d_i^3} \quad (1)$$

Where d_i is the droplet diameter of the i^{th} size class and n_i is the number of droplets of diameter d_i.

$$span = \frac{d_{90} - d_{10}}{d_{50}} \quad (2)$$

Where d_x is the droplet diameter corresponding to x% volume on the cumulative droplet size distribution curve.

Results are the average of at least 4 measurements of 2 independent samples.

2.6.3. ζ-potential

The surface charge of the emulsion droplets was measured using a Zetasizer Nano ZS (Malvern Instruments, Worcestershire, UK) at 25 °C. Emulsions were diluted in deionized water. The refractive index of the dispersant was set to 1.33. The ζ-potential was calculated using the Smoluchowski model.

2.6.4. Oil loss

The centrifugal stability of HIPEs, expressed in term of oil loss (OI) after the centrifugation was determined according to Galvão et al. (2022), by placing around 1 g of emulsion in an Eppendorf tube (previously weighted) and centrifuging at 8600×*g* for 30 min at 4 °C (Biocen 22R, Orto Alresa, Madrid, Spain). After centrifugation, the oil layer was removed using a pipette and the tube containing the emulsion without free oil was weighted. The oil loss was calculated according to Equation (3).

$$\text{OI}\ (\%) = \frac{m_i - m_f}{m_i - m} \tag{3}$$

Where m_i is the initial weight of the Eppendorf with the sample, m_f is the weight of the Eppendorf with the sample after removing the free oil, and m is the weight of the Eppendorf.

2.6.5. Storage stability of HIPEs

The emulsions were placed in tightly closed glass tubes and stored at room temperature (25 °C) for 14 days, protected from light. Storage stability was assessed by determining the changes in visual appearance, droplet size, ζ-potential, and oil loss, on days 0, 7, and 14.

2.6.6. Rheological characteristics

The rheological properties of the HIPEs were characterized at 25 °C in terms of flow behavior and viscoelastic properties using a Discovery HR20 rheometer (TA instruments, New Castle, DE, USA) with a parallel plate geometry (40 mm, 1 mm gap). The rheometer was equipped with a Peltier system for temperature control. All measurements were performed in duplicate for two independent samples for insect protein-stabilized HIPEs. For the WPI-stabilized HIPEs, measurements were conducted in triplicate on a single emulsion, except for the amplitude sweep, which was performed only once. Rheological parameters and yield stress were obtained using Trios™ software (TA instruments, New Castle, DE, USA).

2.6.6.1. Amplitude sweeps. Amplitude sweeps were performed with a strain varying from 0.1 to 100% at a frequency of 10 rad/s, to determine the linear viscoelastic region (LVR). The storage (or elastic) modulus (G') and the loss (or viscous) modulus (G''), as well as the oscillation stress were measured. The values of the yield stress of the HIPEs, expressed in Pa, were obtained as the crossover point of G' and G'' curves when plotted against the oscillation stress (Liu et al., 2019).

2.6.6.2. Frequency sweeps. Frequency sweeps were carried out from 1 to 100 rad/s at a constant strain of 1%, within the LVR identified. The flow behavior was measured over five orders of magnitude in shear rate, ranging from 0.001 to 100 s^{-1} and the apparent viscosity was reported as a function of shear rate.

2.6.6.3. Three-interval thixotropy test (3iTT). During pre-trials, the thixotropic behavior of the HIPEs (i.e., time dependent shear-thinning properties) was verified by performing a thixotropy loop measurement. That is, HIPEs were sheared at ascending shear rate (1–100 or 150 s^{-1}) and then at descending shear rate, each ramp lasting 60 s. The presence of the hysteresis loop area (Fig. S1, in Supplementary materials) showed that the material presented a thixotropic behavior. To further quantify the thixotropic behavior, a three-interval thixotropy test (3iTT) was performed, on selected HIPEs, following a method of Jiang, Li, et al. (2023). First, a shear rate of 0.1 s^{-1} was applied to the sample during 60 s to simulate the state of the emulsion before the 3D printing, then a higher shear rate of 150 s^{-1} was applied during 20 s to simulate the printing process of the emulsion through the nozzle, and finally the shear rate was lowered to 0.1 s^{-1} and maintained during 60 s to simulate the state of the 3D printed emulsion. The viscosity was recorded during the 3 steps. The recovery rate was calculated as the ratio between the viscosity values obtained in the last 10 s of the last interval and the ones obtained in the last 10 s of the first interval.

2.7. 3D printing

Selected HIPEs were printed with a commercial extrusion-based food grade 3D printer (Foodini, Natural Machines Iberia S.L., Barcelona, Spain). Emulsions were printed using a 1.5 mm diameter nozzle at room temperature (25 °C). Based on preliminary studies, the internal parameters of the 3D printer were set as follows: 850 mm/min of printing speed, 2 of ingredient flow speed (dimensionless), 1.4 mm of line thickness, and 1.6 mm of distance between layers. The HIPEs were printed in the shape of a hollow cylinder composed of 3 layers. The printed figures were stored at 4 °C for 9 days to evaluate their storage stability.

Assuming laminar flow within the extrusion's nozzle of the printer, the shear rate applied during the extrusion was calculated using Equation (4). The mass flow was measured from the weight of the printed figure and the time taken to print it, while the emulsion density was used as conversion factor to calculate the corresponding volumetric flow.

$$\dot{\gamma}\left(s^{-1}\right) = \frac{4Q}{\pi \bullet R^3} \tag{4}$$

Where $\dot{\gamma}$ is the shear rate (s^{-1}), Q is the volumetric flow (cm^3/s), and R is the radius of the nozzle (cm).

2.8. Statistical analysis

Results were expressed as mean ± standard deviation. One-way analysis of variance (ANOVA) was performed to determine significant differences ($p < 0.05$) using Minitab 19 statistical software (State College, PA, USA).

3. Results and discussion

3.1. Effect of the thermal treatment on the insect protein dispersions

3.1.1. Protein particle size and ζ-potential

The particle size distribution of LMPC and CPC protein dispersions (untreated, UnT, and thermally treated, ThT) is presented in Fig. 1. Results showed a bimodal distribution for both LMPC-UnT and CPC-UnT; one population of small particles was detected at around 0.500 μm (LMPC-UnT) or 0.250 μm (CPC-UnT) and another one of larger particles was measured at around 10 μm (LMPC-UnT) or 5 μm (CPC-UnT). After thermal treatment, a third large population appeared with particles whose size ranged from around 40 μm–1200 μm for LMPC-ThT and from 35 μm to 550 μm for CPC-ThT, showing that the thermal treatment induced protein aggregation, with bigger aggregates obtained in the case of LMPC.

For both insects, the smallest population (around 0.250–0.500 μm) became more intense after thermal treatment, at the expense of the peak at around 5–10 μm, suggesting that the treatment might also have disrupted smaller size aggregates (Galvão et al., 2023). Pinel et al. (2024) also found a bimodal distribution, when measuring the particle size distribution of mealworm proteins extracted by isoelectric point

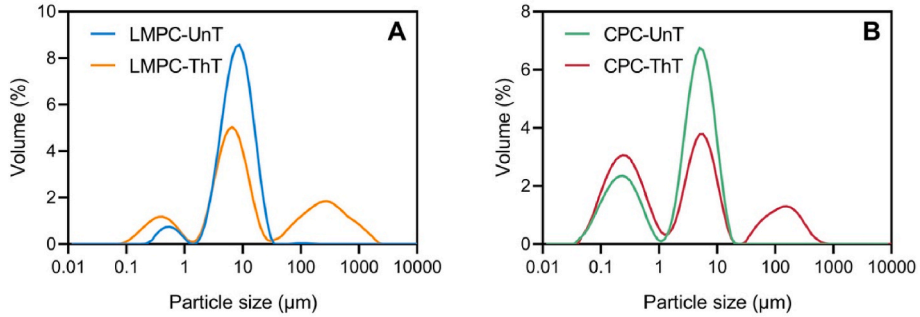

Fig. 1. Particle size distribution of A) LMPC-UnT and LMPC-ThT, and B) CPC-UnT and CPC-ThT. LMPC-UnT: untreated lesser mealworm protein concentrate, LMPC-ThT: thermally-treated lesser mealworm protein concentrate, CPC-UnT: untreated cricket protein concentrate, and CPC-ThT: thermally-treated cricket protein concentrate.

precipitation, with one peak below 1 μm and a peak of larger particles (up to 100 μm). Galvão et al. (2023) found that thermal treatment (70–80 °C for 20 min) of lentil proteins resulted in a reduction of the particle size, with $d_{4,3}$ value decreasing from 57 to 43 μm. However, a thermal treatment accompanied with NaCl addition led to an increase in protein size of Chinese oak silkworm (*Antheraea pernyi*) pupa protein (Ding et al., 2023). Similarly, Mishyna et al. (2019) showed that heat treatment of edible honeybee brood (*Apis mellifera*) at pH 7 caused the formation of aggregates exhibiting higher particle size.

All insect proteins presented a negative ζ-potential (Table 1). The thermal treatment induced a slight increase in the absolute value of ζ-potential for both LMPC (from −26.2 to −30.1 mV) and CPC (from −33.9 to −35.8 mV). The heat induced aggregation of lesser mealworm and house cricket proteins might have led to an increased number of charged groups at the surface of the proteins. A similar behavior has been reported by Liu and Tang (2016) in soy protein after thermal treatment at 90 °C and 100 °C. However, a supplementation in NaCl (100 mM) before a thermal treatment (95 °C, 15 min) of black cricket (*Gryllus assimilis*) protein isolate induced a decrease in the absolute value of ζ-potential, from −36.8 to −28.9 mV (Santiago et al., 2021). Higher absolute value of ζ-potential could contribute to the formation of a more rigid interfacial film and provide sufficient electrostatic repulsion to protect the emulsions against coalescence.

3.1.2. Structural changes: FT-MIR and intrinsic fluorescence

The **FT-MIR** spectra of LMPC-UnT, LMPC-ThT, CPC-UnT and CPC-ThT are presented in Fig. 2. The initial section of the spectra is dominated by a broad band (amide A) in the region 3500–3100 cm^{-1}. Then we can observe two bands, characteristic of protein spectra, the amide I and amide II. The amide I (1700–1600 cm^{-1}) results from C=O stretching, and N-H bending C-N stretching, respectively. These patterns are directly related to the protein backbone conformation, and it has been widely used to understand the protein structure. The amide II band (1600–1500 cm^{-1}) originates mainly from N-H bending and C-H stretching. Even if this band is sensitive to changes in conformation, it has rarely been used (Yang et al., 2015). The spectra did not present major differences before and after thermal treatment. However, slight shifts of the amide bands, especially the shift of the amide I band of

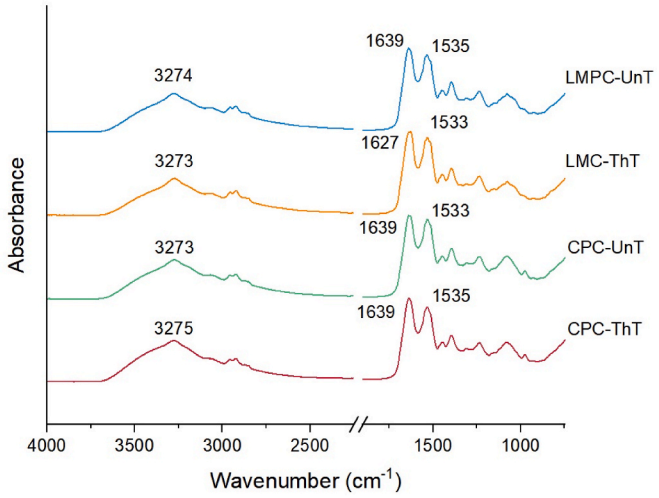

Fig. 2. FT-MIR spectra of LMPC-UnT, LMPC-ThT, CPC-UnT, and CPC-ThT. Notations are as in Fig. 1.

LMPC from 1639 to 1627 cm^{-1} after thermal treatment, suggest changes in secondary structure. Differences in ratio of amide I and amide II bands were observed. LMPC-UnT and LMPC-ThT showed similar amide I/amide II ratio, between 1.08 and 1.09, while CPC-ThT exhibited higher ratio (1.12) than CPC-UnT (1.05). This result indicates that the thermal treatment might have induced differences in secondary and possible tertiary structures of CPC proteins (Ishida & Griffiths, 1993).

The protein secondary structures were analyzed by deconvolution of the amide I band (Table 2). Overall, the proteins had high content of β-sheet (48–60%) and random coil (22–30%) and lower content of α-helix (13–19%) and β-turn (4–6%). The effect of the thermal treatment on the proteins differed between the two insects. The thermal treatment of LMPC induced a significant increase in β-sheet and reduction in random coil, α-helix, and β-turn. In the case of CPC, the heating treatment only impacted the α-helix content which increased significantly.

Table 1
Characteristics of LMPC-UnT, LMPC-ThT, CPC-UnT, and CPC-ThT: ζ-potential and surface hydrophobicity (H_0).

Sample	ζ-potential (mV)	H_0 (−)
LMPC-UnT	-26.2 ± 1.4^{a}	186.9 ± 14.5^{bc}
LMPC-ThT	-30.1 ± 0.7^{b}	219.5 ± 25.5^{c}
CPC-UnT	-33.9 ± 0.7^{c}	133.2 ± 3.9^{a}
CPC-ThT	-35.8 ± 1.2^{d}	168.8 ± 22.8^{ab}

Different letters within a column indicate significant differences ($p < 0.05$). Notations are as in Fig. 1.

Table 2
Secondary structure content of LMPC-UnT, LMPC-ThT, CPC-UnT, and CPC-ThT.

Samples	Secondary structure content (%)			
	β-sheet	Random coil	α-helix	β-turn
LMPC-unT	50.8 ± 1.8^{a}	27.4 ± 1.7^{b}	16.5 ± 0.7^{bc}	5.3 ± 0.3^{b}
LMPC-ThT	60.0 ± 2.2^{b}	21.5 ± 0.5^{a}	14.2 ± 1.7^{ab}	4.4 ± 0.4^{a}
CPC-unT	51.4 ± 0.8^{a}	29.8 ± 0.9^{b}	13.0 ± 0.4^{a}	5.7 ± 0.3^{bc}
CPC-ThT	48.2 ± 3.2^{a}	26.7 ± 3.9^{ab}	19.0 ± 2.2^{c}	6.2 ± 0.8^{c}

Different lowercase letters within a column indicate significant differences ($p < 0.05$). Notations are as in Fig. 1.

Our results obtained for LMPC are in line with a previous study on the impact of drying on the secondary structure of mealworm proteins. Zhang, Xu, et al. (2022) showed that a heating treatment of mealworm proteins reduced the content of α-helix, random coil, and β-turn, and increased the number of β-sheet structures. FT-MIR data suggest that the thermal treatment caused modification of the protein structure, at a greater extent for LMPC than CPC. Higher content of random coil contributes to the protein flexibility facilitating its adsorption at the oil-water interface and the stabilization of the emulsion (Chen et al., 2017; Pan et al., 2019). Thus, the protein flexibility of LMPC might have been significantly reduced after the thermal treatment which could impair its emulsifying properties.

Changes in tertiary structure of proteins can be assessed by studying the protein **intrinsic fluorescence**. Tryptophan, the major intrinsic fluorophore in proteins, has a high sensitivity to changes in its local environment (e.g., polarity and presence of quenchers). Therefore, by analyzing changes in its emission spectra (shifts, or difference in signal intensity) we can obtain information about changes in the protein tertiary structure. The intrinsic fluorescence spectra of LMPC and CPC dispersions (untreated and thermally treated) are presented in Fig. 3.

For both insects, the thermal treatment induced a reduction in the maximum intensity. A decrease of 25 and 21% of the initial intensity peak was observed for LMPC and CPC, respectively. As discussed in Section 3.1, the thermal treatment led to an increase in particle size suggesting that it induced protein-protein interactions and further aggregation, which might have led to a decrease in fluorescence intensity (Ayala et al., 2020; Hellmann & Schneider, 2019). A slight shift (346–348 nm) was observed after heat treatment of CPC but not for LMPC, indicating that the tryptophan residues of CPC might be exposed to a slightly more hydrophilic environment after treatment. From the results we can hypothesize that upon heating, the proteins partially unfolded inducing the shift of the fluorescence spectrum of CPC and subsequently aggregated causing the decrease in fluorescence intensity.

3.1.3. Surface hydrophobicity

The surface hydrophobicity (H_0) values obtained for the protein dispersions is presented in Table 1. Lesser mealworm protein presented higher H_0 values compared to house cricket protein (187–220 vs. 131–169). The H_0 mean values increased for both insects after thermal treatment, however, the differences were not significant. Mishyna et al. (2019) found that thermal treatment at pH 7 led to an increase in surface hydrophobicity. However, Santiago et al. (2021) reported that the modification of surface hydrophobicity of black cricket (*Gryllus assimilis*) depends on the thermal treatment applied and the presence of NaCl. The surface hydrophobicity of the black cricket proteins increased after thermal treatment in absence of NaCl, while it significantly decreased in presence of NaCl.

Kato and Nakai (1980) suggested that thermal treatment impacts distinct proteins in various ways, either increasing or decreasing surface hydrophobicity depending on the conformational changes induced by the thermal treatment. The thermal treatment of LMPC and CPC might have induced exposure of hydrophobic amino acids previously buried within the proteins. Since the increase was not significant and considering that the particle size was larger for thermally-treated proteins, it is possible that the hydrophobic amino acids exposed might have participated in hydrophobic interactions leading to the formation of aggregates (Voutsinas et al., 1983).

3.2. Stabilization of HIPEs using untreated and thermally-treated insect proteins

3.2.1. Characterization of initial HIPEs

High internal phase emulsions (HIPEs) containing 80 wt% sunflower oil were prepared using aqueous phases containing 0.5, 1.0, 2.0, or 3.0% LMPC-UnT, LMPC-ThT, CPC-UnT, and CPC-ThT. The objective was to assess the feasibility of using insect proteins to stabilize HIPEs and to investigate the effects of the thermal treatment of proteins on the stabilization of HIPEs. The resulting HIPEs were compared with WPI-stabilized emulsions (0.5–3% WPI).

O/W HIPEs were successfully produced at 0.5–3% of CPC-UnT, CPC-ThT, and LMPC-UnT. The HIPEs exhibited excellent self-supporting properties, retaining their shape without flowing, both when the tubes were inverted and after being removed from the tubes (Fig. 4). These findings are consistent with previous studies on HIPEs stabilized with a wide range of protein emulsifiers (Gao et al., 2021). The WPI-stabilized HIPEs presented a creamy texture while insect protein-stabilized HIPEs presented a much firmer texture, showing that insect proteins have a superior ability to structure and increase the viscosity of HIPEs. Similarly, Hinderink et al. (2021) found that HIPEs stabilized with pea protein fractions outperformed those stabilized with WPI in terms of self-supporting characteristics.

No O/W emulsion could be formed when using 0.5 and 1% LMPC-ThT. Indeed, during the addition of oil, the O/W emulsions transitioned to W/O emulsions. These emulsions flowed when the tubes were inverted, and were easily dispersed in sunflower oil, confirming the formation of W/O emulsions (Fig. S2 in Supplementary materials). Thus, the thermal treatment of LMPC impacted the minimum protein concentration required to form an 80 wt% sunflower oil HIPE, which was not the case for CPC.

3.2.1.1. ζ-potential. The surface charge of the droplets can be estimated by measuring the ζ-potential. An absolute value of ζ-potential greater than 30 mV is generally considered sufficient to provide adequate repulsion between droplets. All insect protein-stabilized HIPEs presented a negative surface charge at day 0, ranging from −28.5 to −42.7 mV (Table 3). Emulsions stabilized by CPC (untreated or thermally treated) presented significantly higher absolute value of ζ-potential than the emulsions stabilized with the same protein content of LMPC (untreated or thermally treated)

($p < 0.05$). No clear conclusion can be drawn regarding the impact of thermal treatment of proteins on the surface charge of the emulsions. For each insect protein, at the same protein content used in the emulsion, the

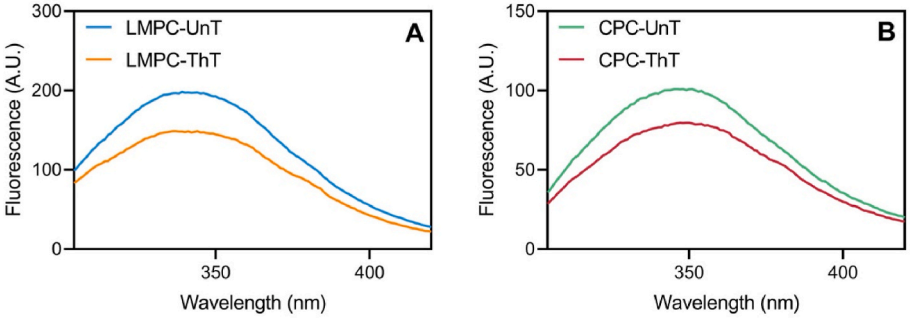

Fig. 3. Intrinsic fluorescence spectra of A) LMPC-UnT and LMPC-ThT, and B) CPC-UnT and CPC-ThT. Notations are as in Fig. 1.

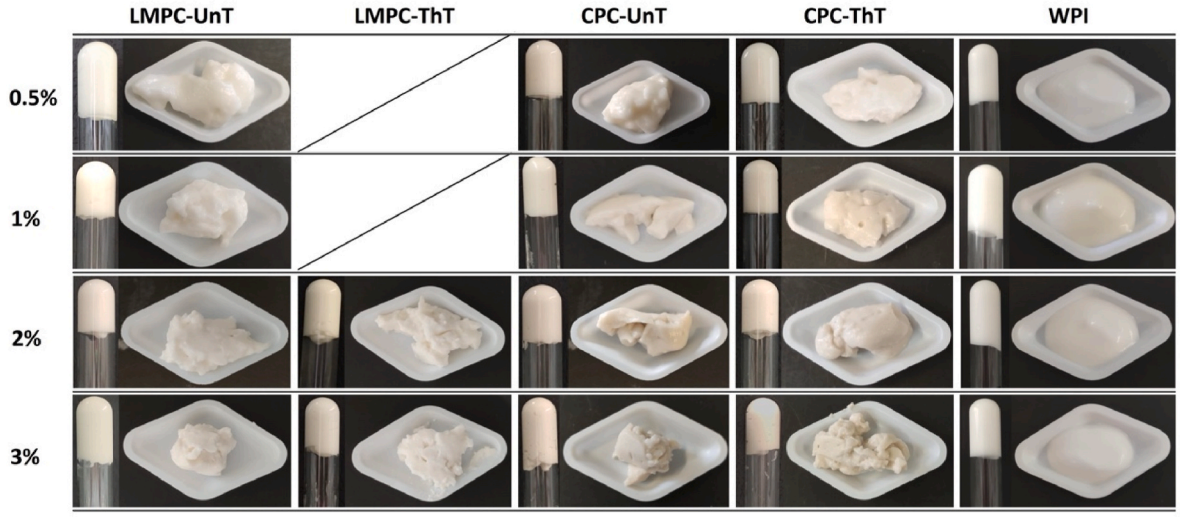

Fig. 4. Visual appearance of HIPEs stabilized with LMPC-UnT, LMPC-ThT, CPC-UnT, CPC-ThT, and WPI. Notations are as in Fig. 1.

Table 3
ζ-potential of the emulsions stabilized with LMPC-UnT, LMPC-ThT, CPC-UnT, CPC-ThT, and WPI at day 0, day 7 and day 14 during storage at 25 °C.

Emulsion	Protein content (%)	ζ-potential (mV)		
		Day 0	Day 7	Day 14
LMPC-UnT	0.5	−32.2 ± 0.8 ab,A	−30.6 ± 1.8 a,A	−31.8 ± 2.0 ab,A
	1.0	−28.5 ± 3.2 a, A	−30.6 ± 1.9 a,AB	−32.4 ± 2.1 ab,B
	2.0	−35.7 ± 2.9 bcde,B	−32.8 ± 1.5 ab,A	−31.6 ± 2.1 a, A
	3.0	−34.7 ± 3.6 bcd,A	−38.0 ± 2.3 cd,B	−34.0 ± 1.5 abc,A
LMPC-ThT	2.0	−33.4 ± 2.1 abc,A	−36.9 ± 2.2 c,B	−35.2 ± 4.1 bcd,AB
	3.0	−40.0 ± 1.2 fg, A	−39.3 ± 2.9 cde,A	−41.4 ± 4.2 f, A
CPC-UnT	0.5	−36.8 ± 3.3 bcdef,A	−37.4 ± 3.4 cd,A	−36.6 ± 4.8 bcde,A
	1.0	−38.2 ± 2.0 def,B	−30.9 ± 2.4 a,A	−38.9 ± 3.3 ef,B
	2.0	−38.3 ± 2.9 def,A	−39.5 ± 3.3 cde,A	−39.4 ± 2.6 ef,A
	3.0	−42.5 ± 2.8 h, B	−43.6 ± 3.0 f,B	−40.2 ± 2.9 ef,A
CPC-ThT	0.5	−32.9 ± 2.4 ab,A	−35.6 ± 2.9 bc,B	−36.8 ± 2.6 cde,B
	1.0	−36.3 ± 1.0 cd,A	−36.3 ± 3.1 c,A	−37.7 ± 1.8 de,A
	2.0	−39.4 ± 1.9 efg,AB	−42.0 ± 3.6 def B	−37.9 ± 3.4 de,A
	3.0	−42.7 ± 1.8 h, A	−41.5 ± 1.6 ef,A	−41.3 ± 3.0 f, A
WPI	0.5	−51.8 ± 1.7 ij, B	−57.5 ± 0.9 I,C	−42.2 ± 1.1 f, A
	1.0	−52.5 ± 1.5 j, B	−54.2 ± 1.0 h,B	−36.5 ± 1.0 bcde,A
	2.0	−42.2 ± 1.7 gh,A	−48.9 ± 3.3 g,B	−50.9 ± 2.4 g, B
	3.0	−47.9 ± 2.9 I, A	−49.1 ± 1.8 g,A	−48.3 ± 3.6 g, A

Different lowercase letters indicate significant differences within a column and different uppercase letters indicate significant differences within a row ($p < 0.05$). Notations are as in Fig. 1.

ζ-potential values were not significantly different, except for the emulsions stabilized with 3% LMPC or 0.5% CPC. HIPEs stabilized with WPI presented initial ζ-potential values from −42.2 mV to −52.2 mV, which were slightly higher than those of insect protein-stabilized HIPEs.

3.2.1.2. Droplet size distribution. The droplet size distribution of insect protein-stabilized HIPEs was measured in both distilled water and 1% SDS solution, as the emulsions were difficult to disperse properly in water. We observed that the droplet distribution sometimes shifted towards lower droplet sizes when measured in SDS solution, indicating weak flocculation of droplets (Fig. 5). Therefore, the droplet size ($d_{4,3}$) and span values reported hereafter are for HIPEs dispersed in SDS solution. WPI-stabilized HIPEs could easily be dispersed in water, and no differences were observed between measurements performed in SDS solution and water (Fig. 5E). Hinderink et al. (2021) also reported weak flocculation of droplets in HIPEs stabilized with whole pea protein or insoluble fractions of pea proteins, whereas HIPEs stabilized with WPI did not exhibit noticeable flocculation.

For all four insect proteins tested, the droplet size distribution shifted towards smaller droplet size with increased protein concentration, likely due to a greater availability of proteins to adsorb at the O/W interface and stabilize the droplets. The $d_{4,3}$ of insect protein-stabilized HIPEs ranged from around 45–58 μm (0.5% protein) to 15–19 μm (3% protein). No peak was observed towards bigger particle size (500–1000 μm) showing that the protein aggregates in the dispersion did not interfere with the measurement.

At low protein concentration, WPI-stabilized HIPEs exhibited smaller droplet size, the emulsions stabilized with 0.5% WPI had a $d_{4,3}$ of around 37 μm. While at higher concentration larger $d_{4,3}$ were obtained (around 26–27 μm for 3% proteins).

The thermal treatment of CPC protein led to lower $d_{4,3}$ for the HIPEs stabilized with 0.5% (44.5 vs. 57.7 μm, for CPC-UnT and CPC-ThT, respectively) and 1% (35.9 vs. 29.6 μm, for CPC-UnT and CPC-ThT, respectively) protein (Fig. 5). At higher protein content, 2 and 3%, no significant differences were found between the untreated and thermally-treated protein for both LMPC and CPC. The span values of the HIPEs varied between 1.0 and 2.1 (Table S1 in Supplementary materials). Generally, a small span (below 1) in O/W emulsions is linked with good storage stability. Nevertheless, higher span values in the range of 1–2 are considered acceptable for HIPEs (Galvão et al., 2022). The presence of smaller oil droplets benefits to the physical stability of the HIPEs, as these droplets can fit between larger droplets, potentially improving the overall physical stability (Zhu et al., 2020).

A wide range of droplet sizes for HIPEs has been reported in the

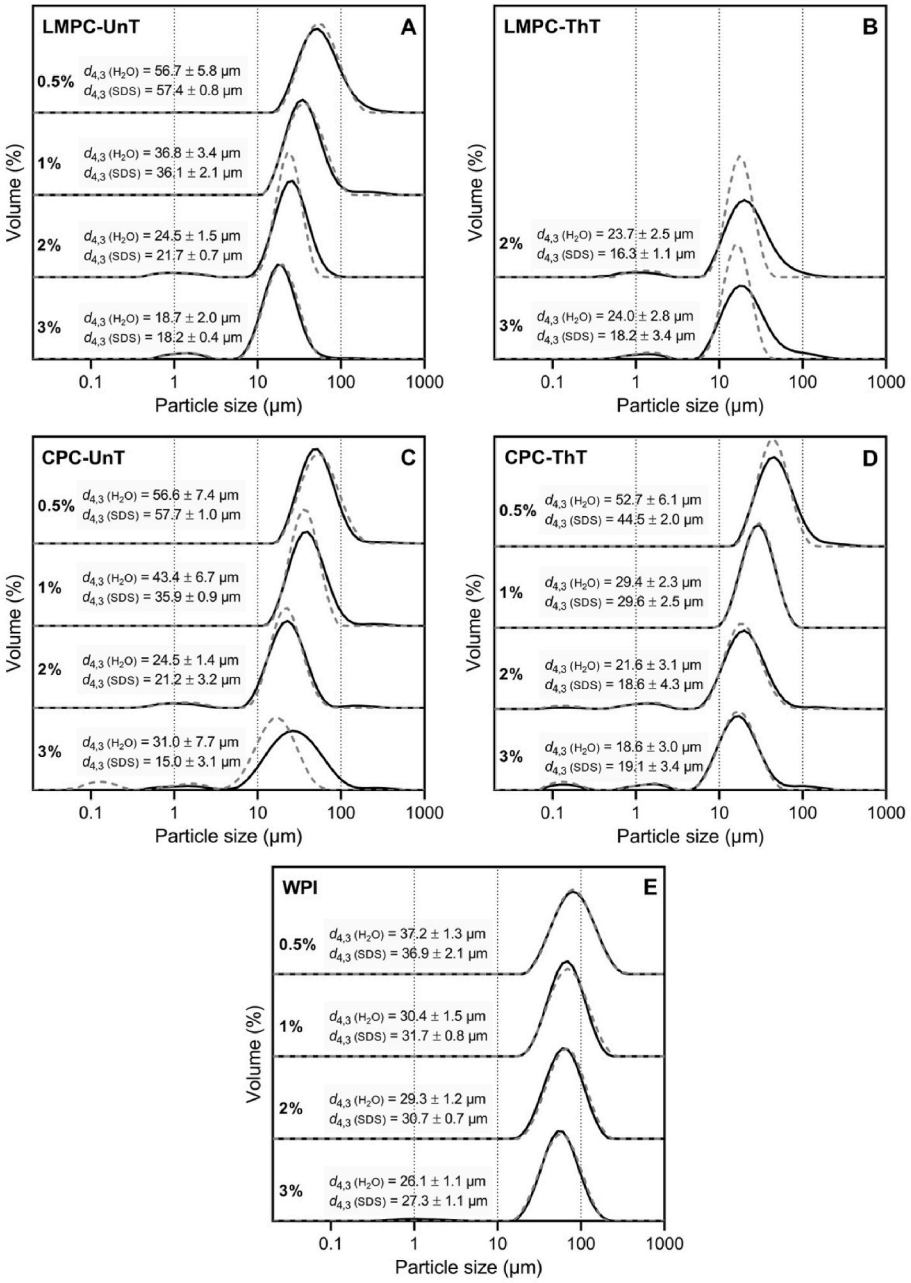

Fig. 5. Droplet size distribution of HIPEs stabilized by A) LMPC-UnT, B) LMPC-ThT, C) CPC-UnT, D) CPC-ThT, and E) WPI, dispersed in distilled water (—) or in 1% SDS (– -). Notations are as in Fig. 1.

literature, from a few micrometers to several hundred micrometers (Zhang et al., 2023). The HIPEs produced in this study had a mean droplet size slightly lower than HIPEs produced using other insect proteins. Jiang, Wang, et al. (2023) reported $d_{4,3}$ in the range of 70–100 µm for 78% (w/w) soybean oil HIPEs stabilized with 2% silkworm pupae protein. Mealworm (*Tenebrio molitor*) proteins were used to stabilize 80% (v/v) corn oil emulsions and the HIPEs obtained presented wider droplet size distribution, with droplets from 20 µm to 300 µm (Huang et al., 2022). It is to be noted that the HIPEs of these studies were dispersed in water and not in SDS solution for the size measurements, thus the diameter obtained could be the diameter of droplet aggregates.

3.2.1.3. Microstructure. The microstructure of the HIPEs stabilized with WPI and insect proteins is presented in Fig. 6. A hexagonal packing of oil droplets is clearly visible which is characteristic of HIPEs and densely packed systems (Zamani et al., 2018). The microscopy images corroborate the droplet size distribution results as we can observe smaller droplets with increased protein contents.

3.2.1.4. Oil loss. The HIPEs were centrifuged to estimate the oil loss. After centrifugation, the samples were separated into 2 or 3 layers, a top layer of oil in some samples, a cream layer, and an aqueous phase. All insect protein-stabilized HIPEs showed no or low oil loss (<1%) at day 0 (Fig. 7). No oil loss was observed for the WPI-stabilized HIPEs as well (data not shown). These results corroborate findings from previous studies exhibiting low oil loss in protein-stabilized HIPEs (Galvão et al., 2023; Morell et al., 2023; Vélez-Erazo et al., 2020).

3.2.2. Storage stability

HIPEs physical stability was studied during 14-day storage at room

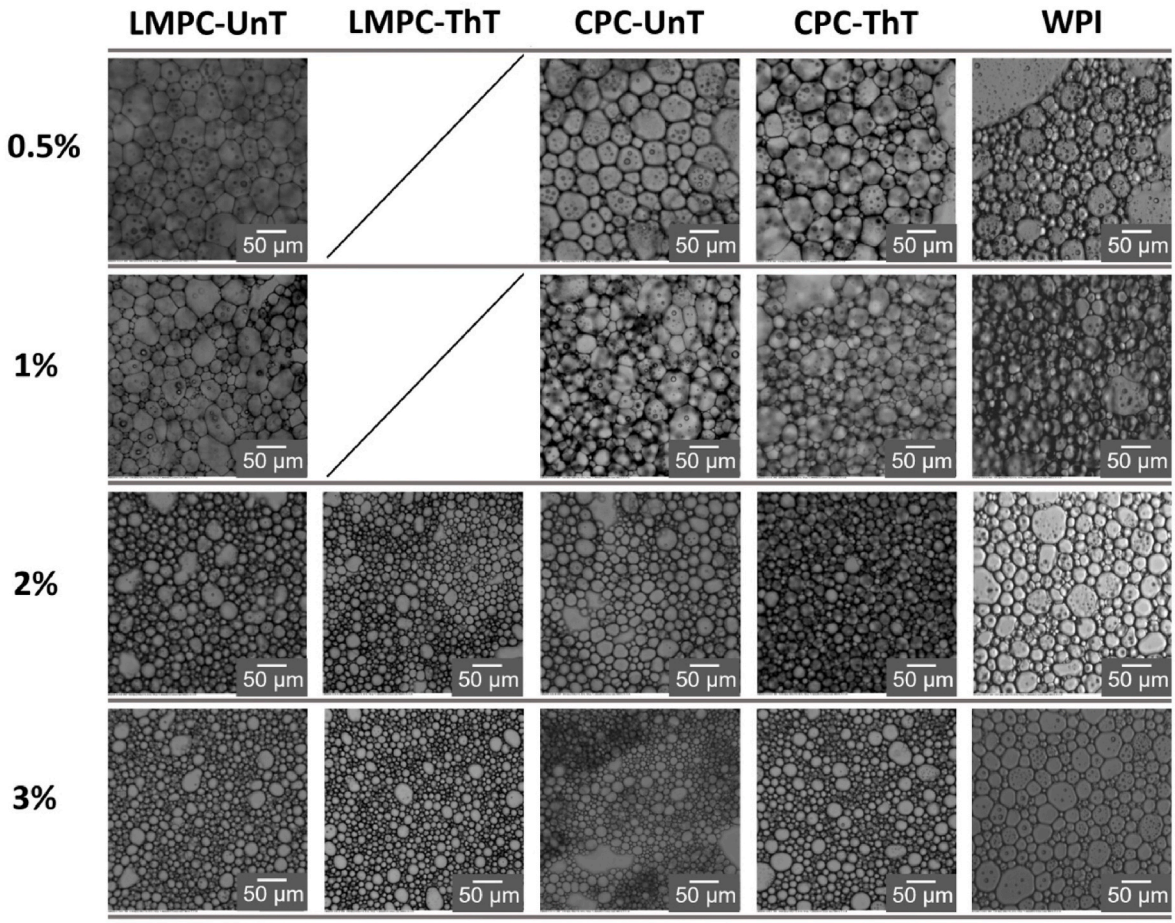

Fig. 6. Microstructure of HIPEs stabilized with LMPC-UnT, LMPC-ThT, CPC-UnT, CPC-ThT, and WPI. Notations are as in Fig. 1.

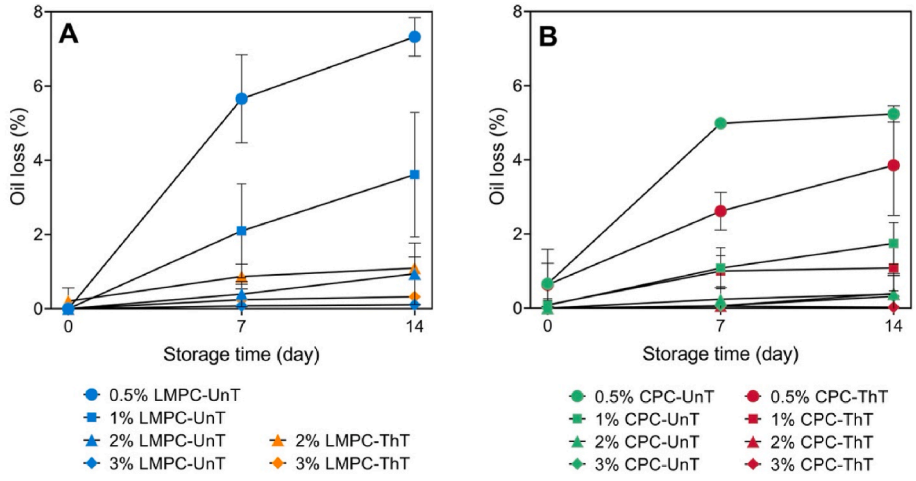

Fig. 7. Oil loss of HIPEs stabilized with A) LMPC-UnT and LMPC-ThT, and B) CPC-UnT and CPC-Th, during 14-day storage at 25 °C. Notations are as in Fig. 1.

temperature (around 25 °C). Overall, all HIPEs produced were highly stable during storage at room temperature, showing no oil layer on the top of the sample. Moreover, all the HIPEs maintained the solid-like appearance and did not flow when tubes were inverted (Fig. 8).

HIPEs stabilized with LMPC-UnT and LMPC-ThT showed slight increase in droplet size after the 14-day storage period (Fig. 9A). Larger increase in $d_{4,3}$ were noted for CPC-UnT and CPC-ThT-stabilized HIPEs (Fig. 9B), but the values stayed within the same range (below 60 μm, apart from HIPEs stabilized using 0.5% CPC-ThT). WPI-stabilized emulsions presented the highest physical stability during the storage with no increase in $d_{4,3}$ (Fig. 9C, $p > 0.05$), at the exception of the HIPEs stabilized with 1% WPI whose droplet size slightly increased.

The surface charge (ζ-potential) of the emulsions is reported in Table 3. The ζ-potential significantly varied during storage for most of the emulsions. Proteins at the interface may undergo conformational rearrangements over time, which can lead to different exposure of charged groups (Wicek & Chibowski, 2002). However, the ζ-potential stayed below −30 mV indicating that there was sufficient repulsion

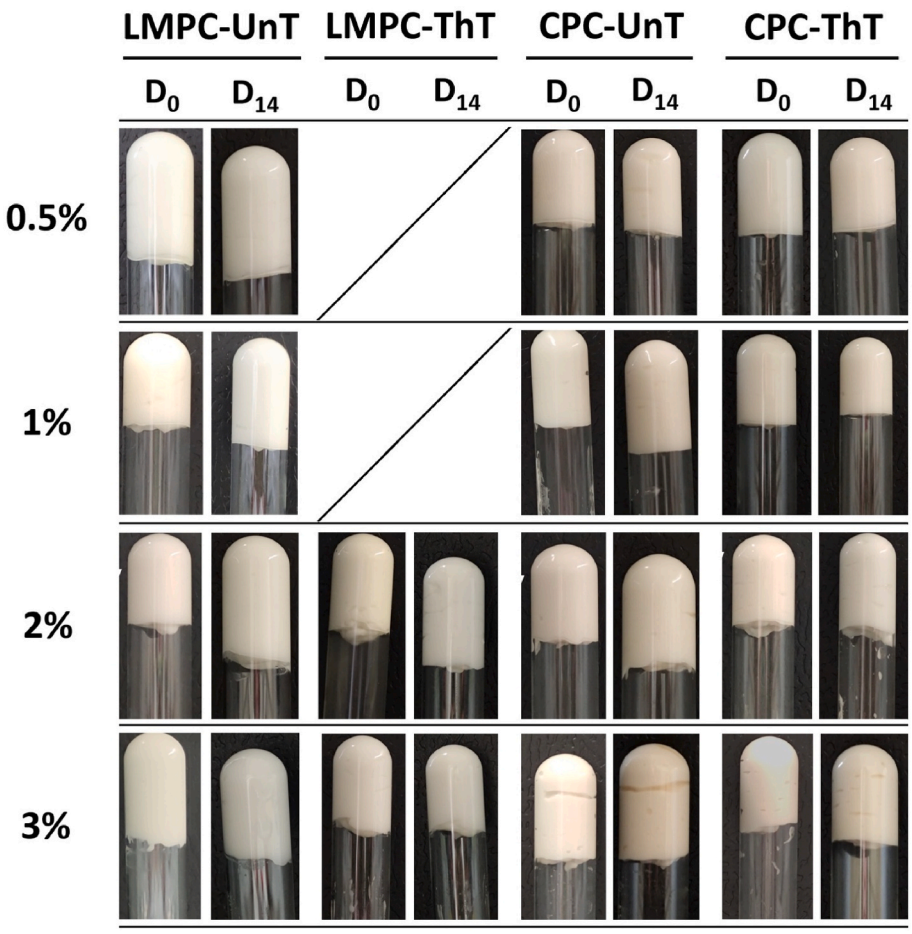

Fig. 8. Visual appearance of HIPEs stabilized with LMPC-UnT, LMPC-ThT, CPC-UnT, and CPC-ThT, at day 0 and after 14 days of storage at room temperature. Notations are as in Fig. 1.

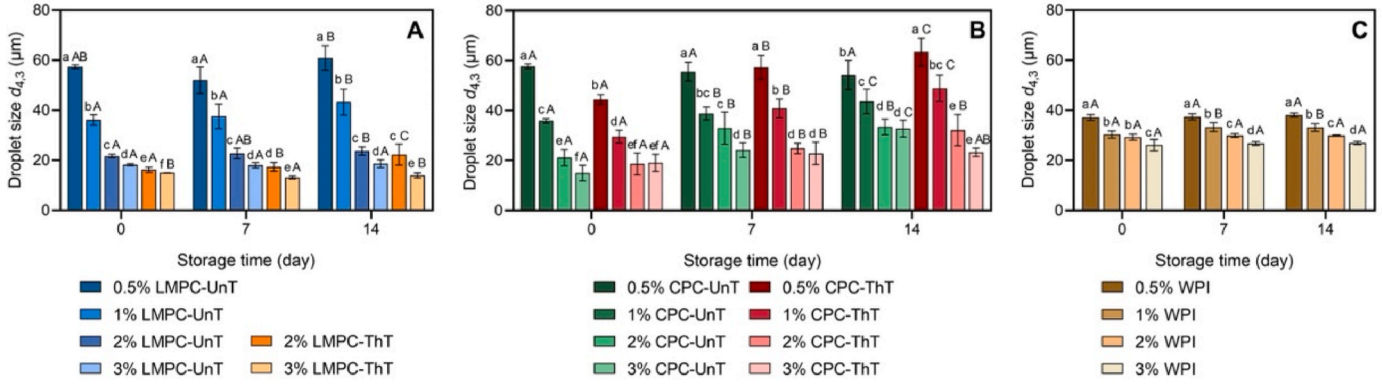

Fig. 9. Droplet size ($d_{4,3}$) of HIPEs stabilized with A) LMPC-UnT and LMPC-ThT, B) CPC-UnT and CPC-ThT, and C) WPI. The reported data correspond to measurements conducted after diluting the insect protein-stabilized HIPEs in 1% SDS solution. WPI-stabilized HIPEs were diluted in water. Different lowercase letters indicate significant differences at the same day of storage and different uppercase letters indicate significant differences at different day of storage for the same emulsifier at the same protein content ($p < 0.05$).

between the droplets during the whole storage period.

The oil loss was measured after 7 and 14 days of storage (Fig. 7). The HIPEs showed low oil loss (below 8%) throughout the whole storage time. Higher oil losses were observed for LMPC-stabilized HIPEs, reaching 7% on day 14 for HIPEs stabilized with 0.5% LMPC-UnT. At low protein concentration (0.5%), the emulsions stabilized with CPC-ThT presented lower oil loss at day 7 and 14 compared to those stabilized with CPC-UnT. The small protein aggregates formed during the thermal treatment of proteins might have helped building a stronger network. WPI-stabilized HIPEs showed great resistance to phase separation as they did not present oil loss up during the whole storage period (data not shown).

Untreated or thermally-treated LMPC and CPC were able to stabilize effectively HIPEs during 14-day storage at room temperature. Other studies have reported similar findings, demonstrating the excellent physical stability of HIPEs stabilized by various proteins (e.g., lentil

proteins, walnut proteins, pea proteins, and gelatin particles) during storage (Galvão et al., 2022; Huang et al., 2023; Zhang et al., 2023).

3.3. Rheological properties of HIPEs

The rheological properties were measured on the emulsions that showed the most promising stability during storage. Consequently, the rheological characterization was only conducted on HIPEs produced with 1%–3% insect protein solutions, as the use of 0.5% protein dispersions resulted in higher oil loss during 14-day storage. WPI-stabilized HIPEs showed a creamy consistency, even at the highest protein concentration tested (3%), that did not seem appropriate for 3D printing. According to this, HIPEs were produced with higher concentration of WPI in the aqueous phase (4–5%) to assess if the HIPEs produced exhibited more adequate rheological properties to be used as food-ink.

A suitable material for extrusion-based 3D printing should be able to flow through the nozzle while also maintaining its shape once deposited on the surface. To assess the potential printability of the selected HIPEs, we carried out the following rheological tests to predict the behavior of HIPEs throughout the three printing stages: flow sweep, to evaluate the viscosity and shear-thinning behavior (extrusion stage); strain sweep, to determine the LVR, yield stress, and the viscoelastic characteristics (extrusion stage); three-interval thixotropy test, to assess whether the ink viscosity is recovered after a stress is applied (recovery stage); and frequency sweep, to analyze how the ink could respond to the addition of layers, and predict shape retention (self-support stage).

3.3.1. Viscosity and shear-thinning behavior

The apparent viscosity of the HIPEs as function of the shear rate is shown in Fig. 10. All HIPEs presented a decrease in viscosity with increasing shear rate, demonstrating shear-thinning behavior characteristic of pseudoplastic fluids. HIPEs produced with a wide range of emulsifiers also showed similar shear-thinning properties (Hinderink et al., 2021; Jiang, Wang, et al., 2023). Such behavior might be attributed to the disruption of weak links formed between droplets, leading to the alignment of the droplets in the flow. This reduces internal resistance and facilitates smoother flow, thereby decreasing the apparent viscosity under higher shear conditions (Hinderink et al., 2021).

This rheological behavior is essential for extrusion-based 3D printing, as it enables the extrusion of viscous material through the nozzle. The material's viscosity must decrease during printing when higher shear rate is applied to facilitate a smooth flow and increase once the material is deposited onto the surface to maintain structural integrity.

The viscosity varied as a function of the protein type and protein concentration. Higher protein concentrations were linked to increased viscosity across the shear rates studied. Smaller droplet sizes were obtained with increasing protein concentrations (as seen in Section 3.2.1), which likely led to a more compact droplet arrangement forming a stronger network (Welch et al., 2006). The higher concentration of unabsorbed proteins may also increase the viscosity of the continuous phase and promote interactions between droplets contributing to strengthen the network.

Insect protein-stabilized HIPEs showed higher viscosity than WPI-stabilized HIPEs. At low shear rates (0.1 s^{-1}), viscosity ranged from

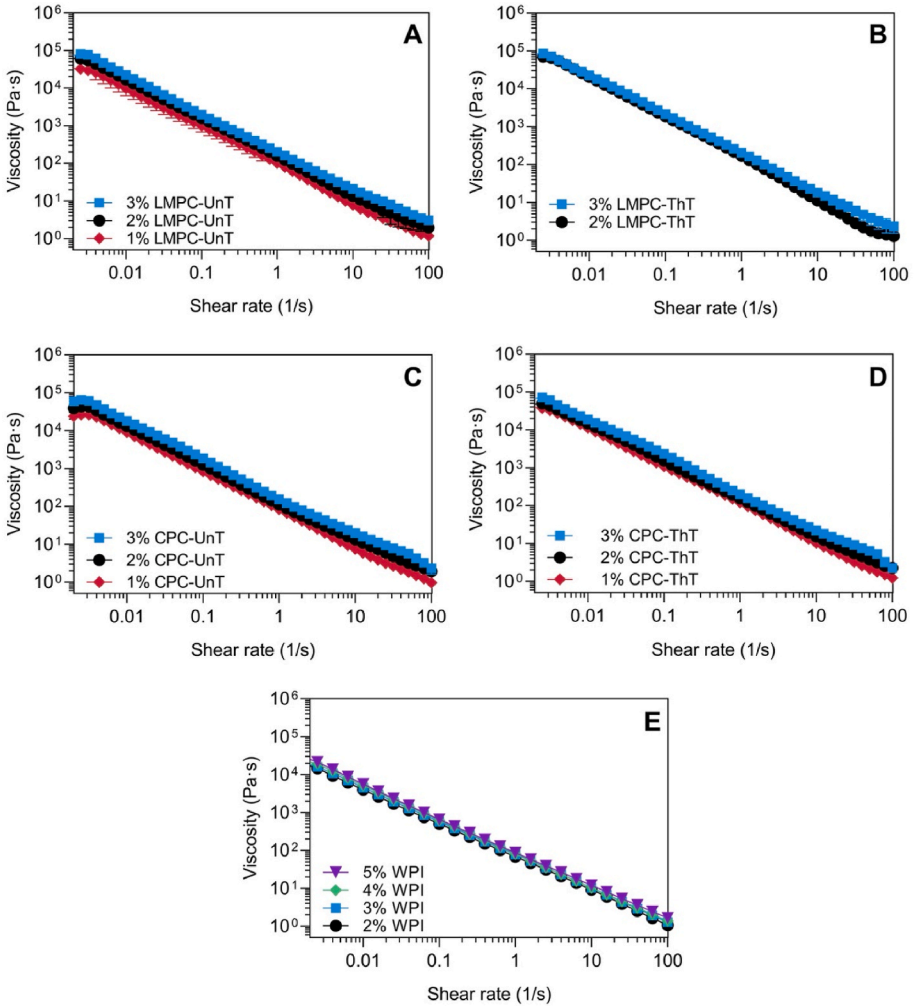

Fig. 10. Flow curves of HIPEs stabilized with A) LMPC-UnT, B) LMPC-ThT, C) CPC-UnT, D) CPC-ThT, and E) WPI. Notations are as in Fig. 1.

502.5 to 654.9 Pa·s for WPI-stabilized emulsions and from 779 to 2300 Pa·s for insect protein-stabilized emulsions. Droplets in insect protein-stabilized HIPEs showed stronger interactions than the ones present in the WPI-stabilized emulsions, as demonstrated by the presence of droplet flocs (see Section 3.2.1), which could explain the higher viscosity. Similar findings were reported by Hinderink et al. (2021), who observed that pea protein-stabilized HIPEs, with weakly flocculated droplets, had higher apparent viscosity than WPI-stabilized HIPEs. The HIPEs produced in the present study presented similar values as HIPEs formulated with silkworm pupa proteins (Jiang, Wang, et al., 2023), with viscosity values around 100–300 Pa·s at shear rate of 1 s^{-1}, at 25 °C.

No clear differences could be observed between the insect protein-stabilized HIPEs from the flow curves. Thus, the power-law model ($\eta = k\dot{\gamma}^{(n-1)}$) was used to fit the apparent viscosity (η) versus shear rate ($\dot{\gamma}$) data. The parameters k is known as the consistency index. It represents the viscosity of the fluid at a shear rate of 1 s^{-1}. Essentially, k is a measure of the fluid's thickness or resistance to flow, with higher values indicating a more viscous (thicker) fluid. The parameter n is the flow behavior index. It describes the degree of pseudoplasticity in the material, indicating whether the behavior is shear-thickening ($n > 1$), Newtonian ($n = 1$), or shear-thinning ($n < 1$). For shear-thinning material, a smaller n value corresponds to higher pseudoplasticity (García et al., 2024). In 3D printing applications, a low k and n are desirable to obtain a smooth and continuous flow of ink through the nozzle (Liu et al., 2019). However, if the consistency is too thin, the nozzle may drip when not printing.

The values of k and n of the HIPEs are presented in Table 4. Across all samples, increasing protein concentration was linked with increased k values. WPI-stabilized HIPEs generally had lower k values than insect protein-stabilized HIPEs, except for HIPEs stabilized with 5% WPI, which exhibited k values comparable to those stabilized with 1% CPC-UnT. When compared at the same protein concentration, k values were higher for LMPC-UnT-stabilized HIPEs (106–201 Pa·s^n) than for CPC-UnT stabilized HIPEs (82–170 Pa·s^n). The thermal treatment of CPC increased the k values to 113–209 Pa·s^n. However, no significant differences in k values were observed between LMPC-UnT and LMPC-ThT-stabilized HIPEs. These findings suggest that WPI-stabilized HIPEs are less thick (or viscous) than insect protein-stabilized HIPEs, which is consistent with the visual appearance of the emulsions (Fig. 4). The thermal treatment of proteins significantly increased the consistency of CPC-HIPEs, resulting in values similar to LMPC-HIPEs.

The n values of all the HIPEs were less than 1 and close to 0 for insect-protein stabilized HIPEs, confirming their strong shear-thinning behavior. The values of n of WPI-stabilized HIPEs were higher than those of insect proteins-stabilized HIPEs, suggesting that HIPEs stabilized with insect proteins have higher degree of pseudoplasticity and better extrudability (Liu et al., 2019). Increase in protein concentration seemed to be linked with a reduction of the absolute value of the n value, in LMPC-stabilized HIPEs. Zhou et al. (2022) suggested that lower protein concentration in protein-stabilized HIPEs was associated with higher shear-thinning behavior because of the reduced surface area of droplets leading to fewer interdroplet interactions.

Table 4
Flow parameters (k and n) and yield stress of HIPEs stabilized with LMPC-UnT, LMPC-ThT, CPC-UnT, CPC-ThT, and WPI.

Sample	k (Pa·s^n)	n (−)	Yield stress (Pa)
1% LMPC-unT	106.0 ± 5.5 ^{f}	−0.040 ± 0.005 ^{e}	105.1 ± 38.3 ^{a}
2% LMPC-unT	139.1 ± 8.8 ^{d}	−0.025 ± 0.002 ^{de}	246.3 ± 12.2 ^{c,d}
3% LMPC-unT	201.0 ± 6.8 ^{ab}	−0.009 ± 0.004 ^{cd}	378.2 ± 20.5 ^{f,g}
2% LMPC-ThT	155.6 ± 7.7 ^{d}	−0.076 ± 0.030 ^{f}	331.2 ± 15.3 ^{e}
3% LMPC-ThT	194.6 ± 6.0 ^{b}	−0.046 ± 0.010 ^{e}	399.1 ± 12.1 ^{g}
1% CPC-unT	81.7 ± 9.7 ^{g}	−0.018 ± 0.016 ^{cde}	139.8 ± 9.2 ^{a}
2% CPC-unT	120.4 ± 1.7 ^{e}	−0.016 ± 0.006 ^{cde}	225.0 ± 2.9 ^{b,c}
3% CPC-unT	170.0 ± 5.8 ^{c}	−0.016 ± 0.005 ^{cde}	339.4 ± 13.7 ^{e,f}
1% CPC-ThT	113.3 ± 6.3 ^{ef}	0.003 ± 0.014 ^{c}	185.0 ± 9.4 ^{b}
2% CPC-ThT	152.8 ± 7.1 ^{d}	−0.003 ± 0.007 ^{cd}	271.2 ± 3.3 ^{d}
3% CPC-ThT	208.9 ± 9.8 ^{a}	−0.004 ± 0.015 ^{cd}	395.6 ± 28.4 ^{g}
2% WPI	68.5 ± 9.6 ^{h}	0.129 ± 0.011 ^{a}	60.5[a]
3% WPI	77.2 ± 4.9 ^{gh}	0.125 ± 0.004 ^{ab}	69.5[a]
4% WPI	80.3 ± 8.1 ^{g}	0.105 ± 0.022 ^{b}	76.3[a]
5% WPI	87.7 ± 3.1 ^{g}	0.119 ± 0.009 ^{ab}	84.3[a]

Different letters within a column indicate significant differences ($p < 0.05$). Notations are as in Fig. 1.

[a] The amplitude sweep was only performed once for the WPI-stabilized HIPEs.

3.3.2. Yield stress

Amplitude sweeps were conducted to determine the linear viscoelastic region (LVR) for each emulsion. The LVR represents the region where the viscoelastic functions (G' and G'') are independent of the strain applied. All HIPEs exhibited a linear regime at low strain values, where the storage modulus (G') was higher than the loss modulus (G'') (Fig. 11). Thus, a solid-like behavior is predominant at low strains. Insect protein-stabilized HIPEs presented a broader LVR compared to WPI-stabilized HIPEs. For WPI-stabilized HIPEs, G' began to decrease at around 3% strain, whereas for insect protein-stabilized HIPEs, this decrease occurred at around 20% strain. This difference may be attributed to the stronger attractive forces between droplets in insect protein-stabilized HIPEs, which led to the formation of droplet flocs as seen in Section 3.2.1 (Hinderink et al., 2021). Additionally, in WPI-stabilized HIPEs, G'' decreased at strains above 30%.

However, insect protein-stabilized HIPEs exhibited first an increase in G'', before decreasing. This behavior could also be attributed to the presence of droplet flocs, which may resist the deformation, leading to the initial increase in G'', until a critical strain is reached, after which G" decreases.

The intersection points between the storage modulus (G') and loss modulus (G'') curves can be used to determine the yield stress, which characterizes the material's static or quasi-static resistance to flow. The yield stress values ranged from 60.5 Pa to 399.1 Pa (Table 4). As expected, and reported by other authors (Li et al., 2020), the yield stress increased with protein concentration, supporting the stronger interactions taking place between droplets at higher protein concentration. WPI-stabilized HIPEs showed the lowest yield stress (60.5–84.3 Pa) among the HIPEs investigated, indicating that insect proteins were more efficient in increasing the stiffness of the system. As for the HIPEs stabilized with LMPC and CPC, no significant differences were observed in yield stress among untreated proteins. The thermal treatment of proteins led to a significant increase in yield stress for both LMPC-(2% protein) and CPC-(2 and 3% protein) stabilized HIPEs, while at 3% protein, the differences between LMPC-UnT and LMPC-ThT-stabilized HIPEs were not significant.

According to Maldonado-Rosas et al. (2022), the yield stress values could be linked to errors during printing, potential deformation, or collapse of the 3D-printed structure. Food formulations with a yield stress in the range of 171.6–484.6 Pa produced structures with minimal errors after being printed using a Foodini 3D printer, the same one used in the present study. Based on this range, we could hypothesize that emulsions stabilized with either 2% or 3% of insect proteins, whether untreated or thermally treated, should be suitable for 3D printing.

3.3.3. Three-interval thixotropy test (3iTT)

A three-interval thixotropy test (3iTT) was performed to evaluate the ability of the HIPEs to recover the viscosity after an extreme shear force (shear rate 150 s^{-1}) that tries to resemble the conditions applied during the 3D printing extrusion stage.

Fig. 12 presents the changes in viscosity of the insect protein-stabilized HIPEs at different shearing rates. Similar trends were observed for all HIPEs. During the first minute, at low shear rate (0.1 s^{-1}) the viscosity of the ink was high (order of magnitude: 103 Pa·s) and stable. When the shear rate was increased to 150 s^{-1}, the viscosity of the

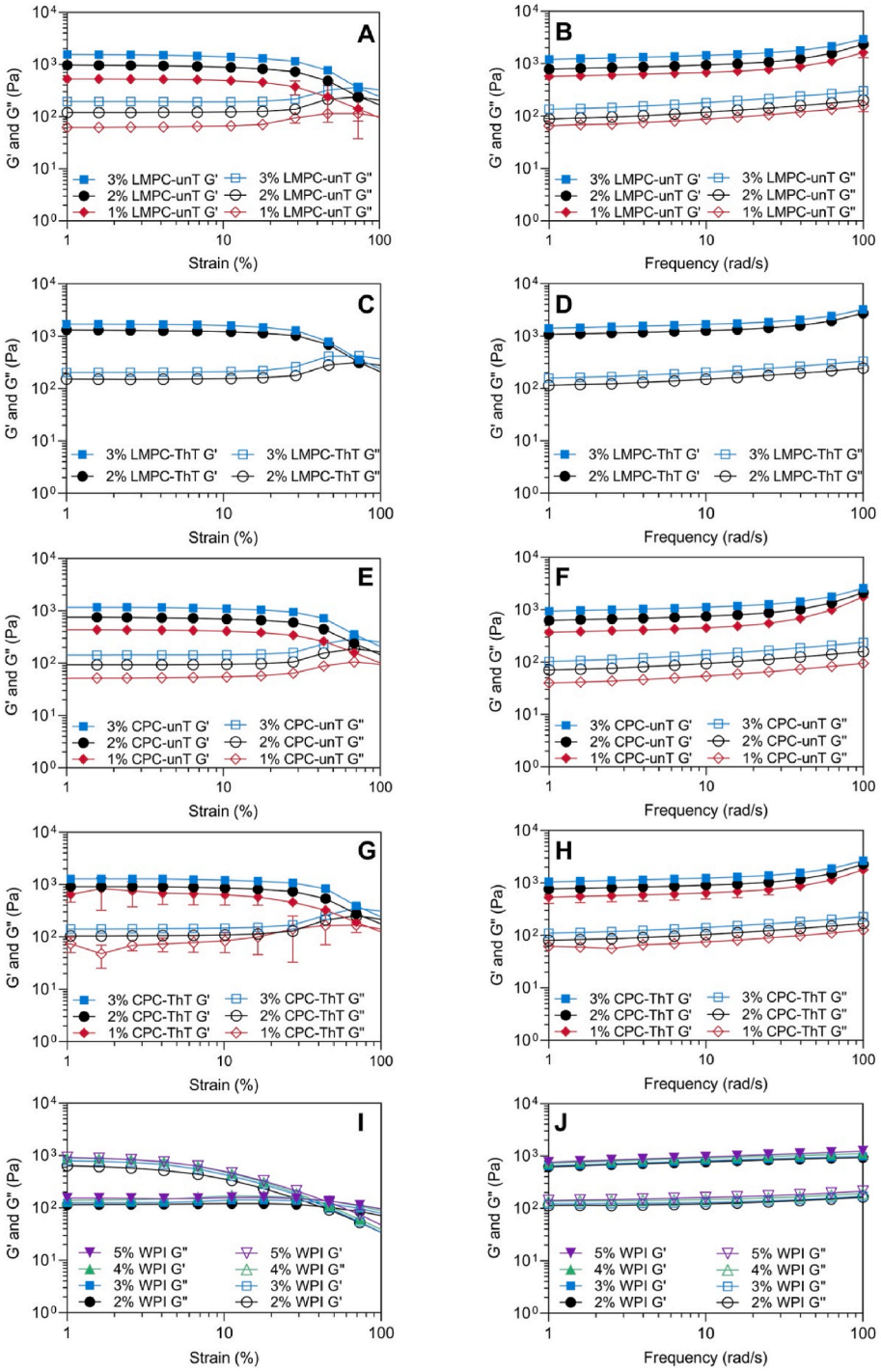

Fig. 11. Rheological profile of HIPEs stabilized with LMPC-UnT, LMPC-ThT, CPC-UnT, CPC-ThT, and WPI. Storage modulus (G', solid symbols) and loss modulus (G'', open symbols) in amplitude sweeps (A, C, E, G, and I) and frequency sweeps (B, D, F, H, and J). Notations are as in Fig. 1.

HIPEs decreased rapidly, which is coherent with the shear-thinning behavior of the HIPEs found previously (see Section 3.3.1). The shear rate was then returned to 0.1 s^{-1}, to evaluate the ability of the HIPEs to restore its network after a stress was applied. All HIPEs recovered quickly from the stress (within few seconds) and showed high viscosity. LMPC-stabilized HIPEs exhibited higher recovery rates (70.6–99.6%) compared to CPC-stabilized HIPEs (63.2–72.5%), with CPC-ThT showing the lowest values. For both insects, the thermal treatment of the proteins seemed to be linked with lower recovery rates, even though the differences were only significant for HIPEs stabilized with 2% LMPC ($p < 0.05$).

The LMPC-stabilized HIPEs presented recovery rates above 70%, for both untreated and thermally-treated proteins which according to Galvão et al. (2022) proved to be high enough to obtain stable structures after the extrusion stage in 3D printing. However, HIPEs stabilized with 2% or 3% of CPC (whether untreated or thermally treated) were less efficient at recovering from the applied stress. In all cases, the initial viscosity was not regained showing that the force applied induced permanent structural changes.

To compare with insect protein-stabilized HIPES, the 3iTT experiment was conducted on HIPEs stabilized with 5% WPI, as they previously showed the highest viscosity of the WPI-stabilized HIPEs. The

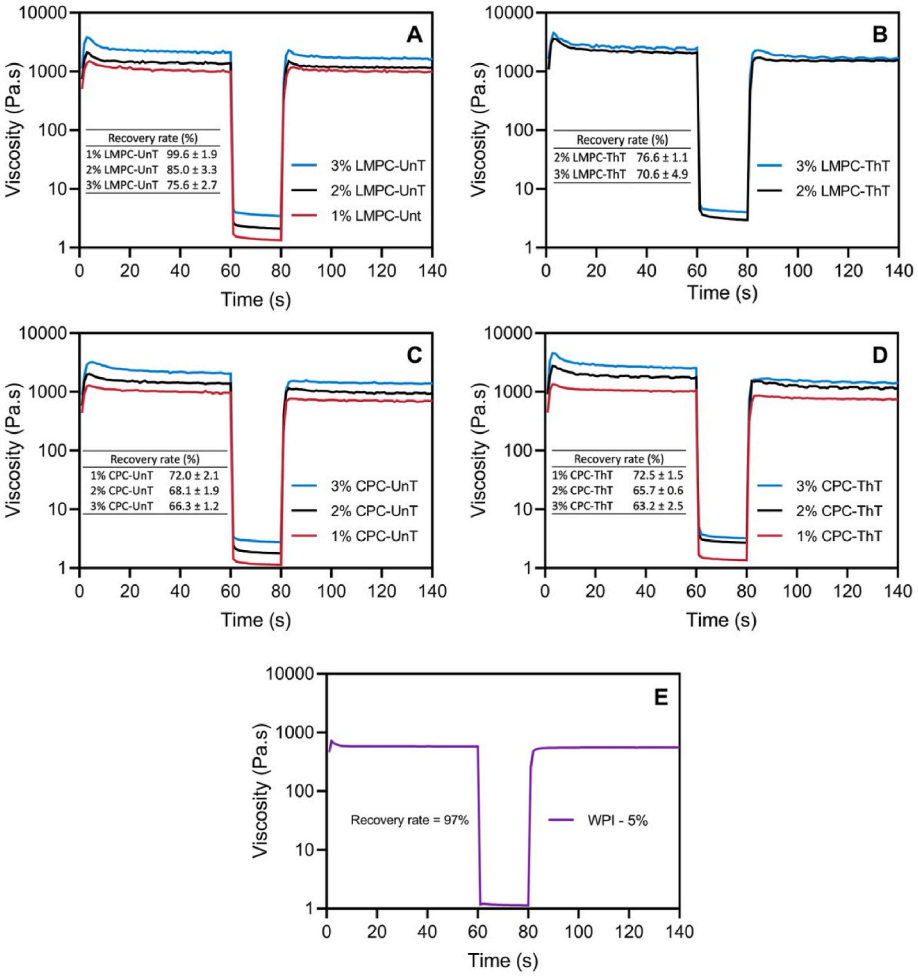

Fig. 12. Three-interval thixotropy test curves of A) LMPC-UnT, B) LMPC-ThT, C) CPC-UnT, D) CPC-ThT, and E) WPI. The recovery rate values are shown in the inserted tables. Notations are as in Fig. 1.

calculated recovery rate was 93.4%, suggesting that WPI-stabilized HIPE network was less damaged during the test. However, despite this higher recovery rate, the viscosity after shearing of WPI-stabilized HIPEs remained lower than that of insect protein stabilized HIPEs. Maldonado-Rosas et al. (2022) reported intermediate recovery values (between 40 and 60%) yet the food formulations still demonstrated good printability and minimal deformation after printing. In addition, for all HIPEs studied in the present work, the viscosity rapidly returned to a stable state after removal of the high shear stress which is suitable in 3D printing.

3.3.4. *Viscoelastic properties*

Oscillatory rheometry was also used to measure the viscoelastic properties of the HIPEs by subjecting them to an oscillating shear strain, at a given amplitude and within a given range of frequencies. This technique provided crucial data essential for understanding the elastic and viscous behavior of the samples across a specified range of oscillatory frequencies or corresponding characteristic times.

The mechanical strength and self-supporting properties of the HIPEs were evaluated by determining the elastic (G') and viscous (G'') modulus during frequency sweep (Tian et al., 2021). The G' of all the HIPEs was higher than the G'' throughout the frequency range studied (Fig. 11), showing a solid-like viscoelastic behavior, which is necessary in 3D printing. Values of G' and G'' were constant with slight increased at higher frequency (>70 rad/s) which is characteristic of soft gels (García et al., 2024).

The values of G', G'', and tan δ (G''/G'), measured at 10 rad/s are presented in Table 5. The storage modulus G' increased with protein concentration indicating that the network formed at higher protein concentration was more elastic. LMPC-UnT exhibited higher values of

Table 5
Viscoelastic parameters of HIPEs stabilized with LMPC-UnT, LMPC-ThT, CPC-UnT, CPC-ThT, and WPI. Storage modulus (G′), loss modulus (G″), and tan δ are reported at 10 rad/s.

Sample	G' (Pa)	G'' (Pa)	tan δ (−)
1% LMPC-unT	679.5 ± 83.0 ^{gh}	87.3 ± 15.8 ^{h}	0.124 ± 0.006 ^{cd}
2% LMPC-unT	941.7 ± 2.5 ^{ef}	117.7 ± 3.01 ^{fg}	0.125 ± 0.003 ^{c}
3% LMPC-unT	1437.5 ± 34.0 ^{b}	180.0 ± 5.4 ^{b}	0.125 ± 0.002 ^{c}
2% LMPC-ThT	1270.0 ± 59.4 ^{c}	149.3 ± 9.8 ^{cd}	0.118 ± 0.002 ^{de}
3% LMPC-ThT	1672.5 ± 80.6 ^{a}	204.3 ± 9.1 ^{a}	0.122 ± 0.002 ^{cd}
1% CPC-unT	449.5 ± 37.2 ^{i}	54.0 ± 4.8 ^{i}	0.120 ± 0.002 ^{cde}
2% CPC-unT	750.3 ± 23.7 ^{g}	94.0 ± 3.8 ^{h}	0.125 ± 0.002 ^{c}
3% CPC-unT	1117.5 ± 32.0 ^{d}	139.3 ± 4.3 ^{de}	0.125 ± 0.002 ^{c}
1% CPC-ThT	556.0 ± 35.4 ^{hi}	63.5 ± 5.7 ^{i}	0.114 ± 0.003 ^{e}
2% CPC-ThT	905.6 ± 29.2 ^{ef}	103.9 ± 4.8 ^{gh}	0.115 ± 0.002 ^{e}
3% CPC-ThT	1237.5 ± 58.5 ^{a}	141.3 ± 7.8 ^{cde}	0.114 ± 0.001 ^{e}
2% WPI	768.3 ± 39.6 ^{g}	122.0 ± 4.4 ^{efg}	0.159 ± 0.003 ^{b}
3% WPI	807.7 ± 14.2 ^{fg}	129.7 ± 3.5 ^{def}	0.161 ± 0.003 ^{ab}
4% WPI	910.7 ± 7.1 ^{ef}	147.7 ± 4.7 ^{cd}	0.162 ± 0.005 ^{ab}
5% WPI	962.3 ± 26.5 ^{e}	161.0 ± 3.6 ^{bc}	0.167 ± 0.002 ^{a}

Different letters within a column indicate significant differences ($p < 0.05$). Notations are as in Fig. 1.

both G' and G'' compared CPC-UnT and WPI. Thermal treatment of LMPC and CPC led to increased G' and G'' values. The values of tan δ were below 1 for all the HIPEs studied, indicating the predominance of the elastic modulus. The values obtained were similar for insect protein-stabilized HIPEs (around 0.12) while they were around 0.16–0.17 for WPI. CPC-ThT stabilized HIPEs had a slightly lower values of tan δ indicating a higher elastic contribution, which could explain the lower recovery rate (Liu et al., 2019; Maldonado-Rosas et al., 2022). Similar values of tan δ (0.1–0.2) were reported for inks printed using Foodini 3D printer (Ekonomou et al., 2024; Riantiningtyas et al., 2021).

3.4. Application of insect protein-stabilized HIPEs as edible ink for 3D printing

Based on rheological analysis, emulsions stabilized with 2% and 3% of LMPC-UnT, LMPC-ThT, CPC-UnT, CPC-ThT, and 5% WPI, were selected as potential food inks. As an initial test of printability, these HIPEs were printed onto a surface using a syringe (Fig. S3 in Supplementary materials). The HIPEs stabilized with 5% WPI failed to retain the line shape adequately as they flowed after being extruded, likely due to the low yield stress (around 80 Pa) and high tan δ (around 0.160). This emulsion was therefore excluded from subsequent experiments performed with the 3D printer.

The potential of LMPC- and CPC-stabilized HIPEs as edible inks, able to function as fat analogues, was further investigated by printing them into the shape of a 3-layer hollow cylinder. Under the selected printing conditions, the shear rate applied during the extrusion with the parameters used in 3D printing was calculated to be 91.7 $\pm$ 1.2 s^{-1}. Although this shear rate is slightly lower than the shear rate applied in the 3iTT (150 s^{-1}), they are in the same order in magnitude providing a reasonable approximation of the actual recovery rate.

Images of the freshly printed figures and those after 9 days of storage at 4 °C are presented in Figs. 13 and 14, for LMPC- and CPC-stabilized HIPEs, respectively. All HIPEs exhibited excellent self-support stability during printing, as the layers did not collapse. This is likely due to the high yield stress (between 255 Pa and 399 Pa) and solid-like behavior of these emulsions. The figures printed with 2% LMPC-UnT and 2% LMPC-ThT presented good definition and smooth edges. However, the figures printed with 3% CPC-UnT and 3% CPC-ThT were not as smooth and presented printing defects. These defects may be attributed to the low recovery rates indicating that the HIPEs may partially lose their structure during printing. In addition, a too high viscosity could lead to uneven extrusion due to the presence of air bubbles within the material for example.

All printed figures maintained their shape even after 9 days of storage at 4 °C showing high self-support properties. The frequency sweep tests indicated that the emulsions possessed strong elastic properties, allowing the printed structures to withstand storage conditions without significant deformation. Overall, the favorable printability displayed by the insect protein-stabilized HIPEs substantiates their potential utilization in food formulations as fat analogues.

4. Conclusions

The outcomes of this investigation prove that lesser mealworm and cricket proteins, whether native or subjected to heat treatment, can be effectively employed to stabilize HIPEs at concentrations of 2–3%. The changes observed following the heat treatment of the proteins in their secondary structure and hydrophobicity do not markedly influence the stabilization of HIPEs. However, it was observed that HIPEs stabilized with thermally-treated proteins exhibited higher viscosity, higher yield stress, and lower recovery rates in comparison to those stabilized with untreated proteins. Furthermore, it was found that insect protein-stabilized HIPEs demonstrated superior self-supporting properties in comparison to WPI-stabilized HIPEs, thus making them more suitable for extrusion-based 3D printing applications. The favorable printability displayed by native and heat-treated lesser mealworm and cricket proteins stabilized HIPEs, and the fact that they keep the shape for nine days under refrigeration, paves the way to their potential utilization in food formulations as fat analogues. Undoubtedly, there are further studies

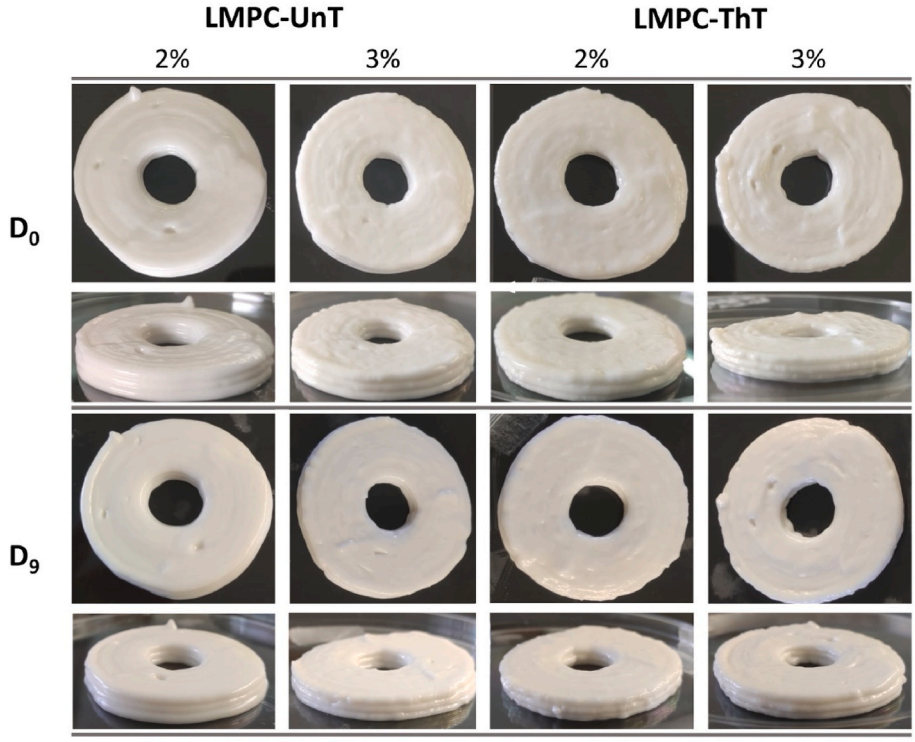

Fig. 13. Images of 3-layer hollow cylinders printed using HIPEs stabilized with 2 and 3% LMPC-UnT and LMPC-ThT, viewed from different directions. The pictures were taken at day 0 and after 9 days of storage at 4 °C. Notations are as in Fig. 1.

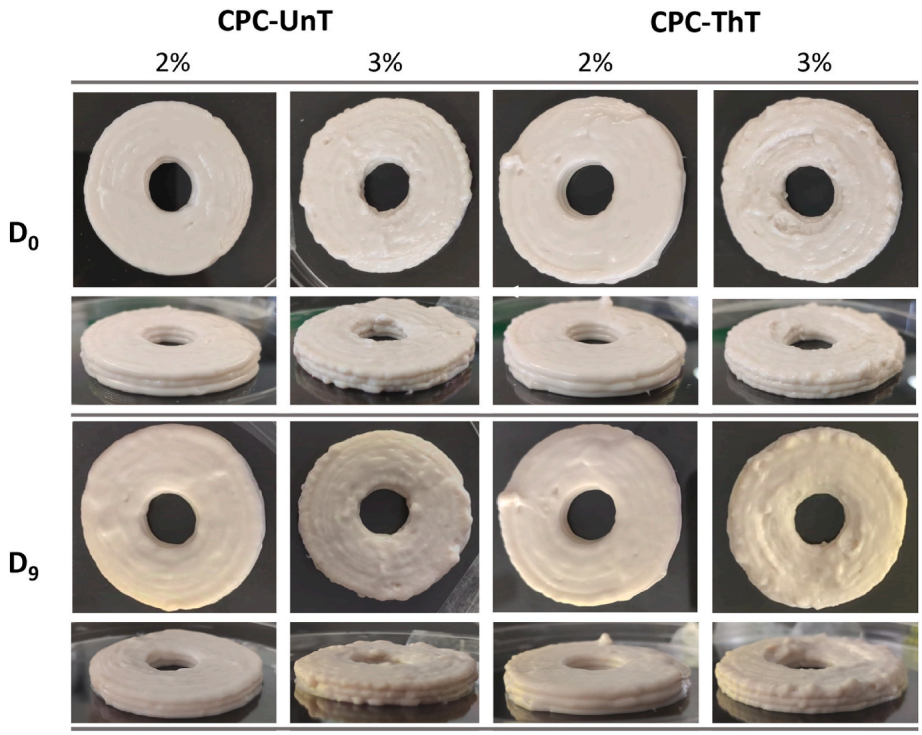

Fig. 14. Images of 3-layer hollow cylinders printed using HIPEs stabilized with 2 and 3% CPC-UnT and CPC-ThT, viewed from different directions. The pictures were taken at day 0 and after 9 days of storage at 4 °C. Notations are as in Fig. 1.

that should be consider, such as the melting behavior of these HIPEs or their potential to incorporate bioactive lipophilic compounds.

CRediT authorship contribution statement

Aurélie Ballon: Writing – original draft, Methodology, Investigation, Conceptualization. **Sarah Sessa:** Investigation. **Salvatore Cito:** Investigation. **Sílvia de Lamo-Castellví:** Resources, Methodology, Funding acquisition, Formal analysis. **Carme Güell:** Writing – review & editing, Resources, Funding acquisition, Formal analysis, Conceptualization. **Montse Ferrando:** Writing – review & editing, Resources, Funding acquisition, Formal analysis, Conceptualization.

Declaration of competing interest

The authors declare that they have no known competing financial interests or personal relationships that could have appeared to influence the work reported in this paper.

Acknowledgments

A. Ballon is grateful for the financial support provided by Generalitat de Catalunya, AGAUR (2022 FI-B2 00010). Graphical abstract was created using BioRender.

Appendix A. Supplementary data

Supplementary data to this article can be found online at https://doi.org/10.1016/j.foodhyd.2025.111330.

Data availability

Data will be made available on request.

References

Abdullah, Weiss, J., Ahmad, T., Zhang, C., & Zhang, H. (2020). A review of recent progress on high internal-phase Pickering emulsions in food science. *Trends in Food Science & Technology, 106*, 91–103. https://doi.org/10.1016/j.tifs.2020.10.016

Ayala, N., Zamora, A., Rinnan, Å., Saldo, J., & Castillo, M. (2020). The effect of heat treatment on the front-face fluorescence spectrum of tryptophan in skim milk. *Journal of Food Composition and Analysis, 92*. https://doi.org/10.1016/j.jfca.2020.103569. Article 103569.

Ballon, A., Romero, M.-P., Rodriguez-Saona, L., de Lamo-Castellví, S., Güell, C., & Ferrando, M. (2024). Conjugation of lesser mealworm (*Alphitobius diaperinus*) larvae protein with polyphenols for the development of innovative antioxidant emulsifiers. *Food Chemistry, 434*. https://doi.org/10.1016/j.foodchem.2023.137494. Article 137494.

Chen, X., Zhou, R., Xu, X., Zhou, G., & Liu, D. (2017). Structural modification by high-pressure homogenization for improved functional properties of freeze-dried myofibrillar proteins powder. *Food Research International, 100*, 193–200. https://doi.org/10.1016/j.foodres.2017.07.007

Czapalay, E., & Marangoni, A. (2024). Functional properties of oleogels and emulsion gels as adipose tissue mimetics. *Trends in Food Science & Technology, 153*. https://doi.org/10.1016/j.tifs.2024.104753. Article 104753.

Ding, Y., Zhao, L., Liu, Y., Sun, J., Pi, Y., & Shao, J.-H. (2023). Effects of protein aggregation induced by NaCl and temperature on gelation of silkworm (*Antheraea pernyi*) pupa raw powder. *International Journal of Biological Macromolecules, 253*. https://doi.org/10.1016/j.ijbiomac.2023.126679. Article 126679.

dos Santos Aguilar, J. G. (2021). An overview of lipids from insects. *Biocatalysis and Agricultural Biotechnology, 33*. https://doi.org/10.1016/j.bcab.2021.101967. Article 101967.

Ekonomou, S., Hadnađev, M., Gioxari, A., Abosede, O. R., Soe, S., & Stratakos, A. C. (2024). Advancing dysphagia-oriented multi-ingredient meal development: Optimising hydrocolloid incorporation in 3D printed nutritious meals. *Food Hydrocolloids, 147*. https://doi.org/10.1016/j.foodhyd.2023.109300. Article 109300.

Fuhrmann, P. L., Breunig, S., Sala, G., Sagis, L., Stieger, M., & Scholten, E. (2022). Rheological behaviour of attractive emulsions differing in droplet-droplet interaction strength. *Journal of Colloid and Interface Science, 607*, 389–400. https://doi.org/10.1016/j.jcis.2021.08.124

Galvão, A. M. M. T., Freitas, J. C., Karatay, G. G. B., Furtado, G. de F., Rasera, M. L., Tavares, G. M., et al. (2023). Thermo-induced changes in the structure of lentil protein isolate (*Lens culinaris*) to stabilize high internal phase emulsions. *International Journal of Biological Macromolecules, 253*. https://doi.org/10.1016/j.ijbiomac.2023.127313. Article 127313.

Galvão, A. M. M. T., Vélez-Erazo, E. M., Karatay, G. G. B., Furtado, G. de F., Vidotto, D. C., Tavares, G. M., et al. (2022). High internal phase emulsions stabilized by the lentil protein isolate (*Lens culinaris*). *Colloids and Surfaces A: Physicochemical*

and Engineering Aspects, 653. https://doi.org/10.1016/j.colsurfa.2022.129993. Article 129993.
Gao, H., Ma, L., Cheng, C., Liu, J., Liang, R., Zou, L., et al. (2021). Review of recent advances in the preparation, properties, and applications of high internal phase emulsions. *Trends in Food Science & Technology, 112*, 36–49. https://doi.org/10.1016/j.tifs.2021.03.041
García, N., Ana, G., Teresa, S., Montse, S., Carme, F., Carmen, G., et al. (2024). Rheological and textural characterisation of chickpea dough and baked 3D - printed snacks enriched with *Alphitobius diaperinus* and *Locusta migratoria* powders. *Food and Bioprocess Technology*. https://doi.org/10.1007/s11947-024-03437-6
Gkinali, A. A., Matsakidou, A., & Paraskevopoulou, A. (2022). Characterization of *Tenebrio molitor* larvae protein preparations obtained by different extraction approaches. *Foods, 11*(23). https://doi.org/10.3390/foods11233852. Article 3852.
Hackshaw, K. V., Yao, S., Bao, H., de Lamo Castellvi, S., Aziz, R., Nuguri, S. M., et al. (2023). Metabolic fingerprinting for the diagnosis of clinically similar long COVID and fibromyalgia using a portable FT-MIR spectroscopic combined with chemometrics. *Biomedicines, 11*(10). https://doi.org/10.3390/biomedicines11102704. Article 2704.
Hellmann, N., & Schneider, D. (2019). Hands on: Using tryptophan fluorescence spectroscopy to study protein structure. *Methods in Molecular Biology*, 379–401. https://doi.org/10.1007/978-1-4939-9161-7_20, 1958.
Hinderink, E. B. A., Schröder, A., Sagis, L., Schroën, K., & Berton-Carabin, C. C. (2021). Physical and oxidative stability of food emulsions prepared with pea protein fractions. *LWT, 146*. https://doi.org/10.1016/j.lwt.2021.111424. Article 111424.
Hu, X., & McClements, D. J. (2022). Construction of plant-based adipose tissue using high internal phase emulsions and emulsion gels. *Innovative Food Science & Emerging Technologies, 78*. https://doi.org/10.1016/j.ifset.2022.103016. Article 103016.
Huang, D., Wu, Y., Li, W., Zhu, X., Liu, J., Jiang, Y., et al. (2022). Advanced insight into the O/W emulsions stabilising capacity of water-soluble protein from *Tenebrio molitor*. *International Journal of Food Science and Technology, 57*(10), 6286–6297. https://doi.org/10.1111/ijfs.15746
Huang, X., Yan, C., Xu, Y., Ling, M., He, C., & Zhou, Z. (2023). High internal phase emulsions stabilized by alkaline-extracted walnut protein isolates and their application in food 3D printing. *Food Research International, 169*. https://doi.org/10.1016/j.foodres.2023.112858. Article 112858.
Ishida, K. P., & Griffiths, P. R. (1993). Comparison of the amide I/II intensity ratio of solution and solid-state proteins sampled by transmission, attenuated total reflectance, and diffuse reflectance spectrometry. *Applied Spectroscopy, 47*(5), 584–589. https://doi.org/10.1366/0003702934067306
Ji, C., & Luo, Y. (2023). Plant protein-based high internal phase Pickering emulsions: Functional properties and potential food applications. *Journal of Agriculture and Food Research, 12*. https://doi.org/10.1016/j.jafr.2023.100604. Article 100604.
Jiang, W., Li, W., Li, J., McClements, D. J., Ma, C., Chen, S., et al. (2023b). High internal phase emulsions stabilized by pea protein isolate-inulin conjugates: Application as edible inks for 3D printing. *Food Hydrocolloids, 142*, Article 108820. https://doi.org/10.1016/j.foodhyd.2023.108820
Jiang, H., Wang, X., Han, L., Tang, C., He, J., & Min, D. (2023). Intestine-targeted high internal phase Pickering emulsion formulated using silkworm pupa protein via ultrasonic treatment. *International Journal of Biological Macromolecules, 246*. https://doi.org/10.1016/j.ijbiomac.2023.125620. Article 125620.
Kato, A., & Nakai, S. (1980). Hydrophobicity determined by a fluorescence probe method and its correlation with surface properties of proteins. *Biochimica et Biophysica Acta, 624*(1), 13–20. https://doi.org/10.1016/0005-2795(80)90220-2
Li, X., Fan, L., Liu, Y., & Li, J. (2023). New insights into food O/W emulsion gels: Strategies of reinforcing mechanical properties and outlook of being applied to food 3D printing. *Critical Reviews in Food Science and Nutrition, 63*(11), 1564–1586. https://doi.org/10.1080/10408398.2021.1965953
Li, X., Xu, X., Song, L., Bi, A., Wu, C., Ma, Y., et al. (2020). High internal phase emulsion for food-grade 3D printing materials. *ACS Applied Materials and Interfaces, 12*(40), 45493–45503. https://doi.org/10.1021/acsami.0c11434
Liu, Z., Bhandari, B., Prakash, S., Mantihal, S., & Zhang, M. (2019). Linking rheology and printability of a multicomponent gel system of carrageenan-xanthan-starch in extrusion based additive manufacturing. *Food Hydrocolloids, 87*, 413–424. https://doi.org/10.1016/j.foodhyd.2018.08.026
Liu, F., & Tang, C. H. (2016). Soy glycinin as food-grade Pickering stabilizers: Part. I. Structural characteristics, emulsifying properties and adsorption/arrangement at interface. *Food Hydrocolloids, 60*, 606–619. https://doi.org/10.1016/j.foodhyd.2015.04.025
Maldonado-Rosas, R., Tejada-Ortigoza, V., Cuan-Urquizo, E., Mendoza-Cachú, D., Morales-de la Peña, M., Alvarado-Orozco, J. M., et al. (2022). Evaluation of rheology and printability of 3D printing nutritious food with complex formulations. *Additive Manufacturing, 58*. https://doi.org/10.1016/j.addma.2022.103030. Article 103030.
Mishyna, M., Martinez, J. J. I., Chen, J., Davidovich-Pinhas, M., & Benjamin, O. (2019). Heat-induced aggregation and gelation of proteins from edible honey bee brood (*Apis mellifera*) as a function of temperature and pH. *Food Hydrocolloids, 91*, 117–126. https://doi.org/10.1016/j.foodhyd.2019.01.017
Morell, P., López-García, A., Hernando, I., & Quiles, A. (2023). Improving pea protein emulsifying capacity by glycosylation to prepare high-internal-phase emulsions. *Foods, 12*(4), 870. https://doi.org/10.3390/foods12040870
Nasrabadi, M. N., Doost, A. S., & Mezzenga, R. (2021). Modification approaches of plant-based proteins to improve their techno-functionality and use in food products. *Food Hydrocolloids, 118*. https://doi.org/10.1016/j.foodhyd.2021.106789. Article 106789.
Palazolo, G. G., Sobral, P. A., & Wagner, J. R. (2011). Freeze-thaw stability of oil-in-water emulsions prepared with native and thermally-denatured soybean isolates. *Food Hydrocolloids, 25*(3), 398–409. https://doi.org/10.1016/j.foodhyd.2010.07.008
Pan, X., Fang, Y., Wang, L., Xie, M., Hu, B., Zhu, Y., et al. (2019). Effect of enzyme types on the stability of oil-in-water emulsions formed with rice protein hydrolysates. *Journal of the Science of Food and Agriculture, 99*(15), 6731–6740. https://doi.org/10.1002/jsfa.9955
Pinel, G., Berthelot, U., Queiroz, L. S., De, L., Santiago, A., Francisco, N., et al. (2024). Influence of the processing on composition, protein structure and techno-functional properties of mealworm protein concentrates produced by isoelectric precipitation and ultrafiltration/diafiltration. *Food Chemistry, 449*. https://doi.org/10.1016/j.foodchem.2024.139177. Article 139177.
Riantiningtyas, R. R., Sager, V. F., Chow, C. Y., Thybo, C. D., Bredie, W. L. P., & Ahrné, L. (2021). 3D printing of a high protein yoghurt-based gel: Effect of protein enrichment and gelatine on physical and sensory properties. *Food Research International, 147*. https://doi.org/10.1016/j.foodres.2021.110517. Article 110517.
Santiago, L. A., Fadel, O. M., & Tavares, G. M. (2021). How does the thermal-aggregation behavior of black cricket protein isolate affect its foaming and gelling properties? *Food Hydrocolloids, 110*, Article 106169. https://doi.org/10.1016/j.foodhyd.2020.106169
Tian, H., Wang, K., Lan, H., Wang, Y., Hu, Z., & Zhao, L. (2021). Effect of hybrid gelator systems of beeswax-carrageenan-xanthan on rheological properties and printability of litchi inks for 3D food printing. *Food Hydrocolloids, 113*, Article 106482. https://doi.org/10.1016/j.foodhyd.2020.106482
van Huis, A., & Oonincx, D. G. A. B. (2017). The environmental sustainability of insects as food and feed. A review. *Agronomy for Sustainable Development, 37*. https://doi.org/10.1007/s13593-017-0452-8. Article 43.
Vélez-Erazo, E. M., Bosqui, K., Rabelo, R. S., Kurozawa, L. E., & Hubinger, M. D. (2020). High internal phase emulsions (HIPE) using pea protein and different polysaccharides as stabilizers. *Food Hydrocolloids, 105*. https://doi.org/10.1016/j.foodhyd.2020.105775. Article 105775.
Voutsinas, L. P., Cheung, E., & Nakai, S. (1983). Relationships of hydrophobicity to emulsifying properties of heat denatured proteins. *Journal of Food Science, 48*(1), 26–32. https://doi.org/10.1111/j.1365-2621.1983.tb14781.x
Wang, J., Ballon, A., Schroën, K., de Lamo-Castellví, S., Ferrando, M., & Güell, C. (2021). Polyphenol loaded $W_1/O/W_2$ emulsions stabilized with lesser mealworm (*Alphitobius diaperinus*) protein concentrate produced by membrane emulsification: Stability under simulated storage, process, and digestion conditions. *Foods, 10*(12), 2997. https://doi.org/10.3390/foods10122997
Wang, J., Jousse, M., Jayakumar, J., Fernández-Arteaga, A., de Lamo-Castellví, S., Ferrando, M., et al. (2021). Black soldier fly (*Hermetia illucens*) protein concentrates as a sustainable source to stabilize O/W emulsions produced by a low-energy high-throughput emulsification technology. *Foods, 10*(5), 1048. https://doi.org/10.3390/foods10051048
Welch, C. F., Rose, G. D., Malotky, D., & Eckersley, S. T. (2006). Rheology of high internal phase emulsions. *Langmuir, 22*(4), 1544–1550. https://doi.org/10.1021/la052207h
Wicek, A. E., & Chibowski, E. (2002). Zeta potential and droplet size of n-tetradecane/ethanol (protein) emulsions. *Colloids and Surfaces B: Biointerfaces, 25*(1), 55–67. https://doi.org/10.1016/S0927-7765(01)00304-6
Wu, C., Liu, Z., Zhi, L., Jiao, B., Tian, Y., Liu, H., et al. (2022). Research progress of food-grade high internal phase pickering emulsions and their application in 3D printing. *Nanomaterials, 12*(17). https://doi.org/10.3390/nano12172949. Article 2949.
Yang, H., Yang, S., Kong, J., Dong, A., & Yu, S. (2015). Obtaining information about protein secondary structures in aqueous solution using Fourier transform IR spectroscopy. *Nature Protocols, 10*(3), 382–396. https://doi.org/10.1038/nprot.2015.024
Zamani, S., Malchione, N., Selig, M. J., & Abbaspourrad, A. (2018). Formation of shelf stable Pickering high internal phase emulsions (HIPE) through the inclusion of whey protein microgels. *Food & Function, 9*(2), 982–990. https://doi.org/10.1039/c7fo01800b
Zhang, M., Li, X., Zhou, L., Chen, W., & Marchioni, E. (2023). Protein-based high internal phase pickering emulsions: A review of their fabrication, composition and future perspectives in the food industry. *Foods, 12*(3). https://doi.org/10.3390/foods12030482. Article 482.
Zhang, J. Y., Pandya, J. K., McClements, D. J., Lu, J., & Kinchla, A. J. (2022). Advancements in 3D food printing: A comprehensive overview of properties and opportunities. *Critical Reviews in Food Science and Nutrition, 62*(17), 4752–4768. https://doi.org/10.1080/10408398.2021.1878103
Zhang, F., Xu, Y., Kong, B., Chen, Q., Sun, F., Zhang, H., et al. (2022). Comparative study of two types of pre-extraction treatment (drying or non-drying) on physicochemical, structural and functional properties of extracted insect proteins from *Tenebrio molitor* larvae. *Current Research in Food Science, 5*, 1570–1580. https://doi.org/10.1016/j.crfs.2022.09.004
Zhou, B., Drusch, S., & Hogan, S. A. (2022). Rheological fingerprinting and tribological assessment of high internal phase emulsions stabilized by whey protein isolate: Effects of protein concentration and pH. *Food Hydrocolloids, 131*, Article 107816. https://doi.org/10.1016/j.foodhyd.2022.107816
Zhu, Y., Huan, S., Bai, L., Ketola, A., Shi, X., Zhang, X., et al. (2020). High internal phase oil-in-water pickering emulsions stabilized by chitin nanofibrils: 3D structuring and solid foam. *ACS Applied Materials and Interfaces, 12*(9), 11240–11251. https://doi.org/10.1021/acsami.9b23430
Zhu, X. F., Zheng, J., Liu, F., Qiu, C. Y., Lin, W. F., & Tang, C. H. (2017). The influence of ionic strength on the characteristics of heat-induced soy protein aggregate nanoparticles and the freeze–thaw stability of the resultant Pickering emulsions. *Food & Function, 8*(8), 2974–2981. https://doi.org/10.1039/c7fo00616k